RSC Advances

PAPER

View Article Online
View Journal | View Issue

Cite this: *RSC Adv.*, 2021, **11**, 25314

Novel pyrimidine-bichalcophene derivatives as corrosion inhibitors for copper in 1 M nitric acid solution

Mai A. Khaled,[ab] Mohamed A. Ismail,[a] Ahmed. A. El-Hossiany[ac] and Abd El-Aziz S. Fouda *[a]

Received 8th May 2021
Accepted 4th July 2021

DOI: 10.1039/d1ra03603c

rsc.li/rsc-advances

This study targets the investigation of three pyrimidine-bichalcophene derivatives (MA-1230, MA-1231, MA-1232) for the prevention of corrosion on copper in 1 M HNO_3 *via* weight loss (WL), potentiodynamic polarization (PDP), and electrochemical impedance spectroscopy (EIS) techniques. The surface morphology was also analyzed by different methods. It was found that the inhibition efficiency (% η) increased by increasing the doses of pyrimidine derivatives and the temperature of the medium. Weight loss data revealed the better adsorption of MA-1232 on the Cu surface at increased inhibitor dose, reaching a maximum efficiency of 99.14% at a dose of 21 μM at 45 °C. The best description of the adsorption of the investigated derivatives on the copper surface was given by the Langmuir isotherm. Some important thermodynamic parameters for the studied inhibitors were computed and are discussed herein. The polarization studies showed that the pyrimidine-bichalcophenes act as mixed inhibitors. Computational chemical approaches were used with informative yields, including quantum-chemical and molecular dynamics simulation techniques, which agree with the experimental results. The results obtained from all tested methods are strongly accepted.

1. Introduction

Copper is among the most widely used metals for industrial and domestic purposes due to its excellent electrical conductivity, good mechanical workability, low cost, and other properties. However, a range of environmental effects can easily cause the corrosion of copper. Nitric acid is the most widely used corrosive solution for copper.[1] Corrosion is an electrochemical process involving anodic and cathodic reactions on the surface of metals.[2] Any alteration in the physical components of metals, due to physicochemical contact with their environments, which results in the deterioration of the metal's character is also called corrosion.[3] Corrosion is expensive, as well as harmful. Every year, billions of dollars are spent on repairing corroded buildings, equipment, and parts. Early failure can lead to the loss of human life and security damage. By adding chemical compounds to a corrodent, the surface metal corrosion can be controlled and minimized. The most effective method for dealing with the corrosion of metals is using inhibitors. A corrosion inhibitor is a substance that, when added in small amounts to the corrosive solution, lowers the corrosion rate of the metal. In recent studies, not only are new inhibitors with high inhibition efficiency being developed, but other characteristics are also considered, such as low-cost, low-toxicity and readiness for production processes.[4] The use of inhibitors is the most practical method for defending against the successive dissolution of metal by corrosion. The use of O, S and N-containing organic compounds to minimize metal corrosion has been studied.[5] The presence of hetero atoms in the inhibitor's chemical structure plays a significant role in the action of corrosion inhibition. Other factors have a significant influence on the efficiency of inhibition, such as molecular weight, aromatic rings, and inhibited metal load.[6–10] Furan and thiophene-containing compounds have been recently reported for their corrosion inhibition effects[11–13] and are described with a wide biological potential range as anticancer agents,[14] antimutagenic agents,[15] and antimicrobial activities.[16] Heterocycle-containing pyrimidine has been found to be a safe inhibitor at concentrations that have excellent corrosion inhibition effects on copper metal in acidic media.[17,18] Some pyrimidine derivatives were utilized as corrosion inhibitors for steel in HCl and H_2SO_4 solutions with their percentage inhibition (% IE) predicted in Table 1. To the authors' best knowledge, pyrimidine-bichalcophene scaffolds have not been evaluated as corrosion inhibitors. In the current study, we evaluated the corrosion inhibition characteristics of three novel pyrimidine-

[a]*Department of Chemistry, Faculty of Science, Mansoura University, Mansoura 35516, Egypt. E-mail: mismail@mans.edu.eg; asfouda@hotmail.com; Fax: +20502202264; Tel: +20502365730*

[b]*Department of Chemistry, Faculty of Dentistry, Horus University, New Damietta, Egypt. E-mail: mkhaled@horus.edu.eg*

[c]*Delta for Fertilizers and Chemical Industries, Talkha, Egypt. E-mail: dr.aselem@hotmail.com*

Table 1 A list of pyrimidine derivatives used for the corrosion inhibition of steel coupons in altered acid medium

Compound	Sample	Medium	% IE	Ref.
(a) 5-(2,5-Dimethylthiophen-3yl)-4-(4-(6-(2,5-dimethylthiophen-3-yl)-2-hydroxypyrimidin-4-yl)phenyl)pyrimidin-2-ol (DTPH) (b) 5-(2,5-Dimethylthiophen-3yl)-4-(4-(6-(2,5-dimethylthiophen-3-yl)-2-mercaptopyrimidin-4-yl)phenyl)pyrimidin-2-thiol (DTPT)	Mild steel	1 M H_2SO_4	85.7, 92.6 respectively at 0.05 mM	19
(a) Benzylidene-pyrimidin-2-yl-amine (b) (4-Methyl-benzylidene)-pyrimidine-2-yl-amine (c) (4-Chloro-benzylidene)-pyrimidine-2-yl-amine	Mild steel	1 M HCl	84.8, 63.2, 75.4 respectively, at 2×10^{-4} M	20
(a) 7-Methoxypyrido[2,3-*d*]pyrimidin-4-amine (MPPA) (b) 4-Amino-7-methoxypyrido[2,3-*d*]pyrimidin-2(1*H*)-one (AMPO)	Mild steel	15% M HCl	86.6, 87.3 respectively at 50 ppm	21
(i) Ethyl(2-amino-5-methyl[1,2,4]-triazolo[1,5-*a*]pyrimidin-7-yl) acetate (ii) Ethyl(5-methyl[1,2,4]triazolo[1,5-*a*]pyrimidin-7-yl)-acetate	Mild steel	1 M HCl	84, 85 respectively at 10^{-3} M	22
D-Glucose derivatives of dihydropyrido-[2,3-*d*:6,5-*d*′]-dipyrimidine-2,4,6,8(1*H*,3*H*,5*H*,7*H*)-tetraone: GPH-3, GPH-2, GPH-1	Mild steel	1 M HCl	97.8, 95.2, 93.9 respectively at 10.15×10^{-5} M	23
3-(2-(4-(Hydroxymethyl)-1*H*-1,2,3-triazol-1-yl)ethyl)-2-methyl-6,7,8,9-tetra-hydropyrido[1,2-*a*] pyrimidin-4-one	Mild steel	1 M HCl	91 at 5 mM	24
(i) 2-((1*E*)-2-Aza-2-pyrimidine-2-ylvinyl)-thiophene (PT) (ii)2-((1*Z*)-1-Aza-2-(2-pyridyl)vinyl)pyrimidine (PP) (iii) 2-((1*E*)-2-Aza-2-(1,3-thiazol-2-yl)vinyl)thiophene (TT) (iv) 2-((1*Z*)-1-Aza-2-(2-thienyl)vinyl)benzothiazole (TBT)	Carbon steel	1 M HCl	57.4, 71.8, 64.4, 49.5 respectively, at 1×10^{-4} M	25

bichalcophene compounds: 5-([2,2′-bifuran]-5-ylmethylene)-1,3-dimethylpyrimidine-2,4,6(1*H*,3*H*,5*H*)-trione (**3a**, MA-1230), 5-([2,2′-bithiophen]-5-ylmethylene)-1,3-dimethylpyrimidine-2,4,6(1*H*,3*H*,5*H*)-trione (**3b**, MA-1231) and 5-([2,2′-bithiophen]-5-ylmethylene)-1,3-diethyl-2-thioxodihydropyrimidine-4,6(1*H*,5*H*)-dione (**3c**, MA-1232). The outcomes indicate that these compounds are brilliant corrosion inhibitors and necessitate further study. In addition to this, considering the actual ecological problems, the interest in these compounds is also highlighted due to their non-toxic characteristics coupled with high solubility in the test solution, which enhance their inhibition efficacy. In this point of view, our aim is to shed more light on the corrosion inhibitive properties of these newly investigated bichalcophene derivatives. Some advanced techniques are used, and surface examination was conducted *via* scanning electron microscopy (SEM) and energy dispersive X-ray (EDX) spectroscopy. Quantum chemical calculations and molecular dynamics simulation were conducted and discussed. The study also portrays the influence of molecular structure on the capability of these molecules to be adsorbed on the metal surface.

2. Experimental procedures

2.1. Materials and solutions

The samples of copper were cut out from a copper sheet with chemical composition (wt%) 0.0023 Pb, 0.005 Zn, 0.0023 P, 0.004 Ni, 0.0018 Al, 0015 Si, 0.0011 S, Co 0.0019, and the rest was Cu. For WL tests, the geometric scale of copper samples was 20–20–2 mm, and for electrochemical measurements, it was 10–10 mm. Prior to the assessment, the samples were abraded with various grades of emery papers (320–2500) till a mirror finish was obtained.

2.1.1. Inhibitors. Three investigated pyrimidine-bichalcophene inhibitors **3a–c** were synthesized as presented in Scheme 1. The chemical structures and molecular formulas are listed in Table 2. The investigations were done at different concentrations (5×10^{-6}, 9×10^{-6}, 13×10^{-6}, 17×10^{-6} and 21×10^{-6} M) in the presence and absence of the investigated inhibitors. All experiments were conducted under thermostatic conditions.

2.1.2. Preparation of pyrimidine-bichalcophene inhibitors 3a–c

*2.1.2.1. 5-([2,2′-Bifuran]-5-ylmethylene)-1,3-dimethylpyrimidine-2,4,6(1H,3H,5H)-trione (**3a**, MA-1230).* A mixture of 1,3-

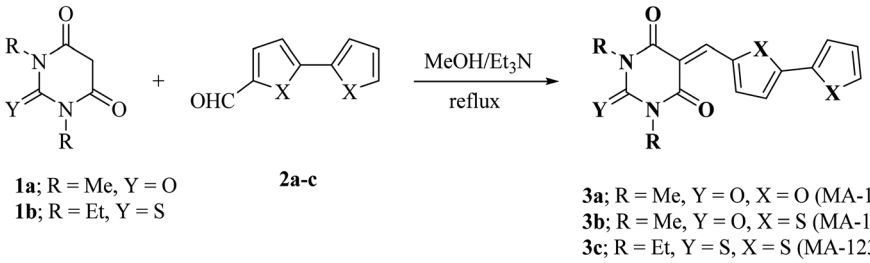

Scheme 1 Synthetic routes of the investigated pyrimidine-bichalcophene derivatives.

Table 2 Molecular structures, formulas, weights of pyrimidine-bichalcophene derivatives

Inhibitor code	Molecular structures/chemical names	Mol formulas (mol. wt.)
(**3a**), MA-1230	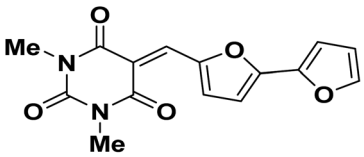 5-([2,2'-bifuran]-5-ylmethylene)-1,3-dimethylpyrimidine-2,4,6(1H,3H,5H)-trione	$C_{15}H_{12}N_2O_5$ (300.27)
(**3b**), MA-1231	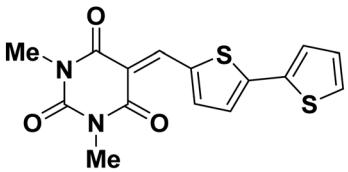 5-([2,2'-Bithiophen]-5-ylmethylene)-1,3-dimethylpyrimidine-2,4,6(1H,3H,5H)-trione	$C_{15}H_{12}N_2O_3S_2$ (332.39)
(**3c**), MA-1232	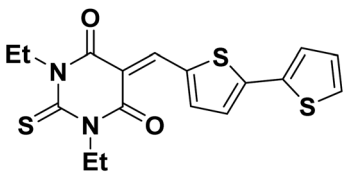 5-([2,2'-bithiophen]-5-ylmethylene)-1,3-diethyl-2-thioxodihydropyrimidine-4,6(1H,5H)-dione	$C_{17}H_{16}N_2O_2S_3$ (376.51)

dimethylbarbituric acid (**1a**) (5 mmol) and 2,2′-bifuran-5-carboxaldehyde[26] **2a** (5 mmol) was refluxed in methanol (30 mL) in the presence of Et_3N (0.5 mL) for 6 h. The precipitate was filtered off, washed with methanol, and recrystallized from DMF/EtOH to afford pyrimidine-bifuran derivative **3a** in 83% yield, mp 249–250 °C. IR (KBr) ν' 3129, 3108 (sp^2 C–H stretch), 2957, 2923 (sp^3 C–H stretch), 1722, 1658 (CO), 1608, 1563, 1534 (C=C) cm^{-1}. ^{1}H-NMR (DMSO-d_6); δ 3.23 (s, 6H; 2× CH_3), 6.75–6.77 (m, 1H), 7.18 (d, $J = 4.0$ Hz, 1H), 7.22 (d, $J = 3.5$ Hz, 1H), 7.97 (d, $J = 1.0$ Hz, 1H), 8.12 (s, 1H), 8.64 (d, $J = 4.0$ Hz, 1H). MS (EI) *m*/*z* (rel. int.); 300 (M^+, 100). Anal. calc. for $C_{15}H_{12}N_2O_5$ (300.27): C, 60.00; H, 4.03; N, 9.33 found: C, 60.17; H, 3.94; N, 9.01%.

*2.1.2.2. 5-([2,2′-Bithiophen]-5-ylmethylene)-1,3-dimethylpyrimidine-2,4,6(1H,3H,5H)-trione (**3b**, MA-1231).* The same procedure used for the preparation of **3a** was adopted using 2,2′-bithiophene-5-carboxaldehyde **2b** (ref. 26) instead of the formyl bifuran derivative **2a** to afford pyrimidine-bithiophene derivative **3b** in 80% yield, mp 240–242 °C, lit.[27] mp not reported. Spectroscopic data not previously reported: IR (KBr) ν' 3094, 3074 (sp^2 C–H stretch), 2953 (sp^3 C–H stretch), 1719, 1649 (CO), 1551, 1520 (C=C) cm^{-1}. MS (EI) *m*/*z* (rel. int.); 332 (M^+, 100).

*2.1.2.3. 5-([2,2′-Bithiophen]-5-ylmethylene)-1,3-diethyl-2-thioxodihydropyrimidine-4,6(1H,5H)-dione (**3c**, MA-1232).* The same procedure used for the preparation of **3a** was employed using 1,3-diethyl-2-thiobarbituric acid (**1b**) instead of compound **1a** and 2,2′-bithiophene-5-carboxaldehyde (**2b**) instead of the formyl bifuran derivative **2a** to afford pyrimidine-bithiophene derivative **3c** in 76% yield, mp 224.5–226 °C. IR (KBr) ν' 3083 (sp^2 C–H stretch), 2978, 2930 (sp^3 C–H stretch), 1686, (CO), 1652, 1552, 1518 (C=C), 1290 (CS) cm^{-1}. ^{1}H-NMR (DMSO-d_6); δ 1.19–1.25 (m, 6H, 2× CH_3 of CH_3CH_2), 4.41–4.48 (m, 4H, 2× CH_2 of CH_3CH_2), 7.21–7.23 (m, 1H), 7.69 (d, $J = 4.0$ Hz, 1H), 7.74 (d, $J = 4.0$ Hz, 1H), 7.79 (d, $J = 4.0$ Hz, 1H), 8.24 (d, $J = 4.0$ Hz, 1H), 8.62 (s, 1H). MS (EI) *m*/*z* (rel. int.); 376 (M^+, 100). Anal. calcd. for $C_{17}H_{16}N_2O_2S_3$ (376.52): C, 54.22; H, 4.28; N, 7.44 found: C, 53.93; H, 4.34; N, 7.21%.

2.2. Weight loss (WL) measurements

The inhibition efficiency of the investigated inhibitors was calculated using eqn (1) when copper coins were pre-weighed and tested in the presence and the absence of these inhibitors in 1 M HNO_3 solution. The samples were removed, dried, and measured after 3 h:[28]

$$\%\ \eta = \theta \times 100 = \left(1 - \left(\frac{W}{W^\circ}\right)\right) \times 100 \quad (1)$$

where W° is the WL value for blank and W is the WL value for the solution with inhibitor.

2.3. Electrochemical techniques

Electrochemical studies were conducted using the Volta-Master 4 software package V7.8 with the Volta-Lab model PGZ402 potentiostat. The potentiostat was attached in the following way to a conventional cell with three electrode arrangements: copper metal as the working electrode (WE), platinum wire as the counter electrode (CE) and the saturated calomel electrode (SCE) as the reference electrode. The measurements started with the immersion of WE in the electrolyte for 1 h to determine the steady state of the open circuit potential (OCP). EIS measurements were measured with an AC signal in the range of frequency between 100 kHz to 0.03 Hz at 10 mV amplitude OCP. PDP measurements were carried out at potentials from −250 mV to +250 mV and at a scan rate of 0.5 mV s^{-1} at controlled temperature. All experimental techniques were performed three times to achieve better data repeatability.

2.4. Surface morphology investigation by SEM and EDX techniques

The metal surface morphology was examined using scanning electron microscopy (SEM) (SEM model JOEL, JSM-T20, Japan) after the immersion of copper coins with and without the highest concentrations of the three pyrimidine derivatives for 24 hours in acid solutions. The copper samples were analyzed using energy dispersive X-ray (EDX) spectroscopy (Zeiss Evo 10 instrument model). The voltage of the accelerating beam was 25 kV.

2.5. Quantum calculations

Gaussian version 4.4.0 used density functional theory (DFT) to measure the quantum chemical parameters and indexes.[29] The quantum parameters associated with corrosion inhibition were calculated, including the energy gap ($\Delta E = E_{LUMO} - E_{HOMO}$), ($I_p$) the ionization ($I_p = -E_{HUMO}$), ($E_A$) the electron affinity ($E_A = -E_{LUMO}$), the dipole moment (debye), the global hardness (η), softness (σ), and chemical potential (μ).

2.6. Quantum Monte Carlo (MC) simulation

MC simulations were performed using Materials Studio program version 7.0 (Accelrys Inc., San Diego, CA, USA) in a simulation box with periodic boundary conditions. The pure copper crystal was adopted and cleaved along the most stable (less energy) plane (1 0 0), constructing a 30 Å vacuum slab. The plane Cu surface of (1 0 0) was relaxed by decreasing its energy, then extending the surface of Cu (1 0 0) to a supercell (10/10). The simulation analysis

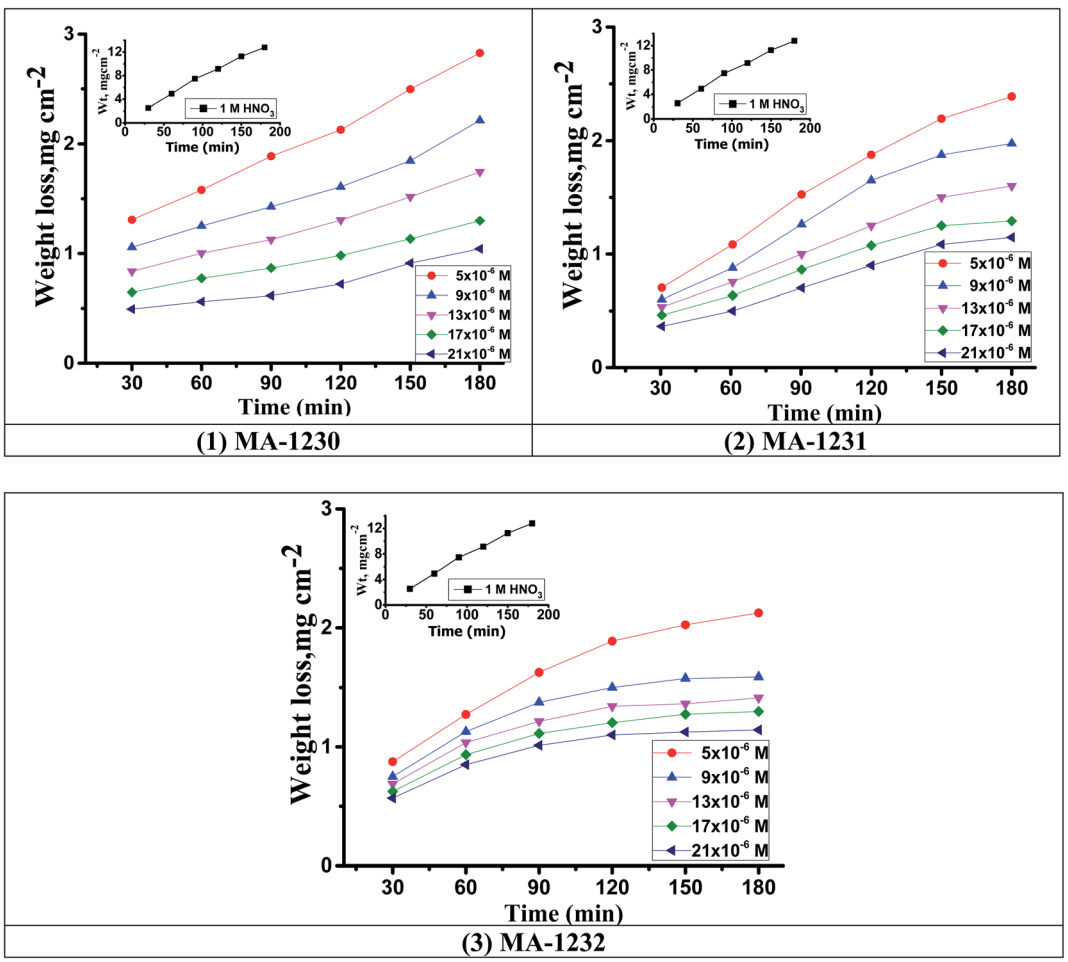

Fig. 1 WL–time curves for the dissolution of copper metal in 1 M HNO_3 at different derivative concentrations (1) MA-1230, (2) MA-1231 and (3) MA-1232 at 25 °C.

was carried out using the MC quest in a test box containing the simulated corrosive species and one molecule of each inhibitor and assigning the high-quality force field known as COMPASS to combine organic parameters and inorganic substances.[30]

3. Results and discussion

3.1. Weight loss (WL) measurements

3.1.1. The effects of concentration and temperature. The effects of the pyrimidine derivatives examined on copper metal corrosion were measured in a solution of 1.0 M HNO_3 using the WL method at 25 °C as in Fig. 1. The temperature effects on inhibition efficiency and corrosion rate (k_{corr}) are demonstrated in Table 3. Fig. 1 illustrates that by increasing the concentration of derivatives, % η_{WL} increases and k_{corr} decreases. Also, by increasing temperature % η_{WL} increases and k_{corr} decreases, indicating that these derivatives are excellent inhibitors at higher temperatures. % η_{WL} increases from (78.24–96.75) at 25 °C to (92.51–99.14) at 45 °C. The increase in % η_{WL} is due to the adsorption of additives on the copper surfaces and this leads to the accumulation of a protective layer on the surface of the Cu[31,32] which increases by increasing the temperature. % η_{WL} of the investigated derivatives are in the order of MA-1232 > MA-1231> MA-1230 at different temperatures.[33]

3.1.2. Thermodynamic activation parameters. There is an agreement that corrosion is related to the Arrhenius equation, noting that by the Arrhenius equation, the activation energy E_a^* is measured by using k_{corr}:[34]

$$\log k_{corr} = \left(\frac{-E_a^*}{2.303RT}\right) + \log A \quad (2)$$

where R is the universal gas constant, T is the absolute temperature, A is the Arrhenius pre-exponential factor and k_{corr} is the corrosion rate. Straight lines were obtained when plotting ($\log k_{corr}$) *versus* ($1/T$) with the intercept of A and slope $E_a^*/2.303R$ for the investigated derivatives as shown in Fig. 2; from this, E_a^* values can be calculated. The data in Table 4 show that on increasing the inhibitor concentration, the E_a^* values decreased, suggesting that the adsorption of these derivatives on the Cu surface is through chemical means.[35–37] The entropy of activation ΔS^* and standard enthalpy ΔH^* are computed from the transition state equation:[38,39]

$$\log k_{corr} = \log\left(\frac{R}{Nh}\right) + \frac{\Delta S^*}{2.303R} + \frac{\Delta H^*}{2.303RT} \quad (3)$$

where N is Avogadro's number and h is Planck's constant. Plots of ($\log k_{corr}/T$) *versus* ($1/T$) for all additives gave straight lines with intercepts of ($\ln(R/Nh) + \Delta S^*/R$) that were used to give the values of ΔS^*, and slopes of ($-\Delta H^*/R$) to obtain the values of ΔH^*, which are listed in Table 4. Fig. 3 shows transition state for the three additives. ΔH^* values are positive and this is

Table 3 % η and k_{corr} of the inhibitors at different concentrations calculated from WL measurements for copper metal at various temperatures

		MA-1230		MA-1231		MA-1232	
Temp, °C	Conc., μM	k_{corr}, mg cm^{-2} min^{-1}	% η	k_{corr}, mg cm^{-2} min^{-1}	% η	k_{corr}, mg cm^{-2} min^{-1}	% η
25	Blank	0.052 ± 0.0012	—	0.052 ± 0.0013	—	0.052 ± 0.0012	—
	5	0.015 ± 0.0023	75.05	0.015 ± 0.0015	79.51	0.008 ± 0.0021	92.63
	9	0.012 ± 0.0015	78.04	0.014 ± 0.0012	81.97	0.008 ± 0.0023	92.74
	13	0.018 ± 0.0018	79.04	0.016 ± 0.0026	86.34	0.009 ± 0.0026	92.84
	17	0.017 ± 0.0009	81.04	0.016 ± 0.0020	88.25	0.009 ± 0.0023	95.32
	21	0.019 ± 0.0029	78.24	0.052 ± 0.0023	89.21	0.008 ± 0.0038	96.75
30	Blank	0.089 ± 0.0020	—	0.089 ± 0.0020	—	0.089 ± 0.0020	—
	5	0.012 ± 0.0020	76.05	0.013 ± 0.0017	84.05	0.008 ± 0.0018	93.07
	9	0.012 ± 0.0009	79.28	0.009 ± 0.0020	89.06	0.007 ± 0.0020	94.67
	13	0.015 ± 0.0023	81.08	0.012 ± 0.0023	93.60	0.007 ± 0.0020	95.39
	17	0.018 ± 0.0017	84.10	0.013 ± 0.0026	94.18	0.007 ± 0.0029	95.85
	21	0.016 ± 0.0020	85.92	0.031 ± 0.0026	94.30	0.006 ± 0.0023	96.47
35	Blank	0.101 ± 0.0017	—	0.101 ± 0.0017	—	0.101 ± 0.0017	—
	5	0.011 ± 0.0015	80.13	0.0137 ± 0.0002	86.52	0.008 ± 0.0015	93.17
	9	0.012 ± 0.0020	80.96	0.009 ± 0.0020	89.22	0.007 ± 0.0023	94.87
	13	0.012 ± 0.0021	89.15	0.012 ± 0.0026	94.70	0.006 ± 0.002333	95.85
	17	0.014 ± 0.0017	85.29	0.013 ± 0.0015	94.87	0.005 ± 0.0017	96.47
	21	0.013 ± 0.0023	94.22	0.031 ± 0.0023	95.04	0.005 ± 0.0018	97.10
40	Blank	0.137 ± 0.0020	—	0.137 ± 0.0020	—	0.137 ± 0.0020	—
	5	0.010 ± 0.0020	80.90	0.010 ± 0.0018	88.18	0.007 ± 0.0017	94.61
	9	0.011 ± 0.0018	82.20	0.005 ± 0.0020	90.45	0.006 ± 0.0020	95.32
	13	0.011 ± 0.0026	89.33	0.006 ± 0.0020	95.15	0.005 ± 0.0020	95.98
	17	0.012 ± 0.0023	91.03	0.006 ± 0.0023	95.91	0.003 ± 0.0023	97.23
	21	0.012 ± 0.0020	91.40	0.027 ± 0.002	95.98	0.004 ± 0.0023	98.11
45	Blank	0.151 ± 0.0015	—	0.151 ± 0.0015	—	0.151 ± 0.0015	—
	5	0.009 ± 0.0017	81.96	0.008 ± 0.0027	89.23	0.006 ± 0.0015	92.74
	9	0.011 ± 0.0017	83.15	0.005 ± 0.0023	93.57	0.005 ± 0.0015	95.92
	13	0.009 ± 0.0020	91.26	0.006 ± 0.0023	94.32	0.004 ± 0.0017	96.32
	17	0.011 ± 0.0018	91.89	0.005 ± 0.0017	97.24	0.002 ± 0.0017	97.36
	21	0.010 ± 0.0015	92.51	0.012 ± 0.0018	97.45	0.001 ± 0.0010	99.14

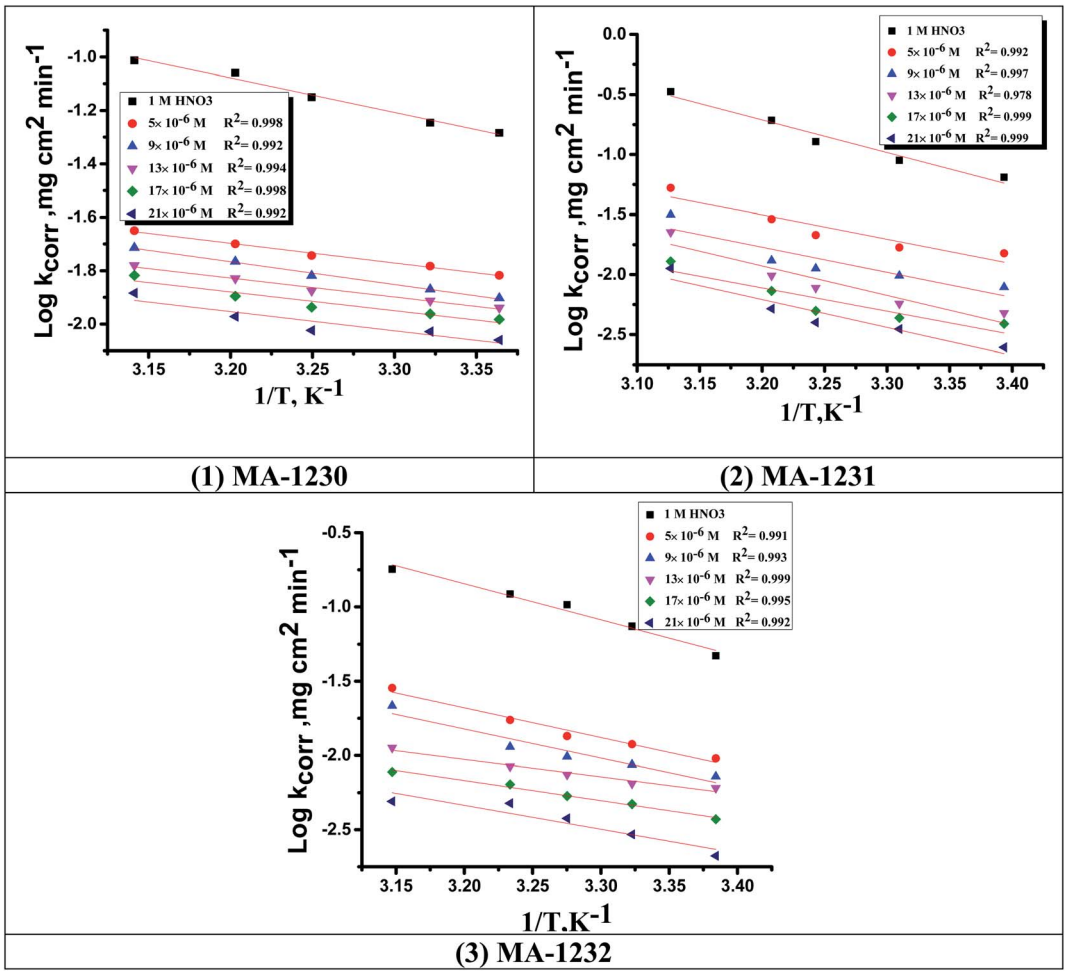

Fig. 2 Arrhenius plots for Cu corrosion in the 1 M HNO_3 solution of inhibitors (1) MA-1230, (2) MA-1231, and (3) MA-1232.

a reference that the copper metal dissolution is an endothermic process[40,41] and confirms the chemical adsorption of these derivatives on the Cu surface. With increasing concentration of additives, the sign of ΔS^* is negative indicating that at the rate determining step of the activated complex, there is association rather than dissociation.[42,43]

Table 4 Activation parameters for copper metal corrosion in 1 M HNO_3 solution without and with various concentrations of inhibitors

		Activation parameters		
Inhibitor	Conc., $\times 10^6$ M	E_a^*, kJ mol^{-1}	ΔH^*, kJ mol^{-1}	$-\Delta S^*$, J mol^{-1} K^{-1}
Free acid (1 M HNO_3)		68.7 ± 0.2028	88.2 ± 0.2603	175 ± 0.2404
MA-1230	5	18.5 ± 0.2309	13.5 ± 0.2309	234 ± 0.1528
	9	13.7 ± 0.2028	17.4 ± 0.2603	223 ± 0.2333
	13	13.6 ± 0.20278	15.0 ± 0.1732	232 ± 0.2309
	17	13.4 ± 0.2603	12.8 ± 0.2333	240 ± 0.2729
	21	12.7 ± 0.2333	11.0 ± 0.2404	252 ± 0.1453
MA-1231	5	47.1 ± 0.1732	40.9 ± 0.1453	143 ± 0.1453
	9	44.4 ± 0.2028	40.0 ± 0.2028	151 ± 0.1764
	13	38.9 ± 0.1732	50.3 ± 0.2028	121 ± 0.1528
	17	38.2 ± 0.2603	40.9 ± 0.2333	154 ± 0.1732
	21	37.1 ± 0.2646	35.8 ± 0.1732	173 ± 0.1764
MA-1232	5	38.3 ± 0.2028	23.2 ± 0.2333	206 ± 0.1856
	9	37.4 ± 0.1528	23.2 ± 0.2309	216 ± 0.1764
	13	30.8 ± 0.2028	19.5 ± 0.2603	223 ± 0.1528
	17	25.9 ± 0.2603	21.1 ± 0.2333	221 ± 0.1453
	21	22.45 ± 0.2048	27.0 ± 0.1764	206 ± 0.2646

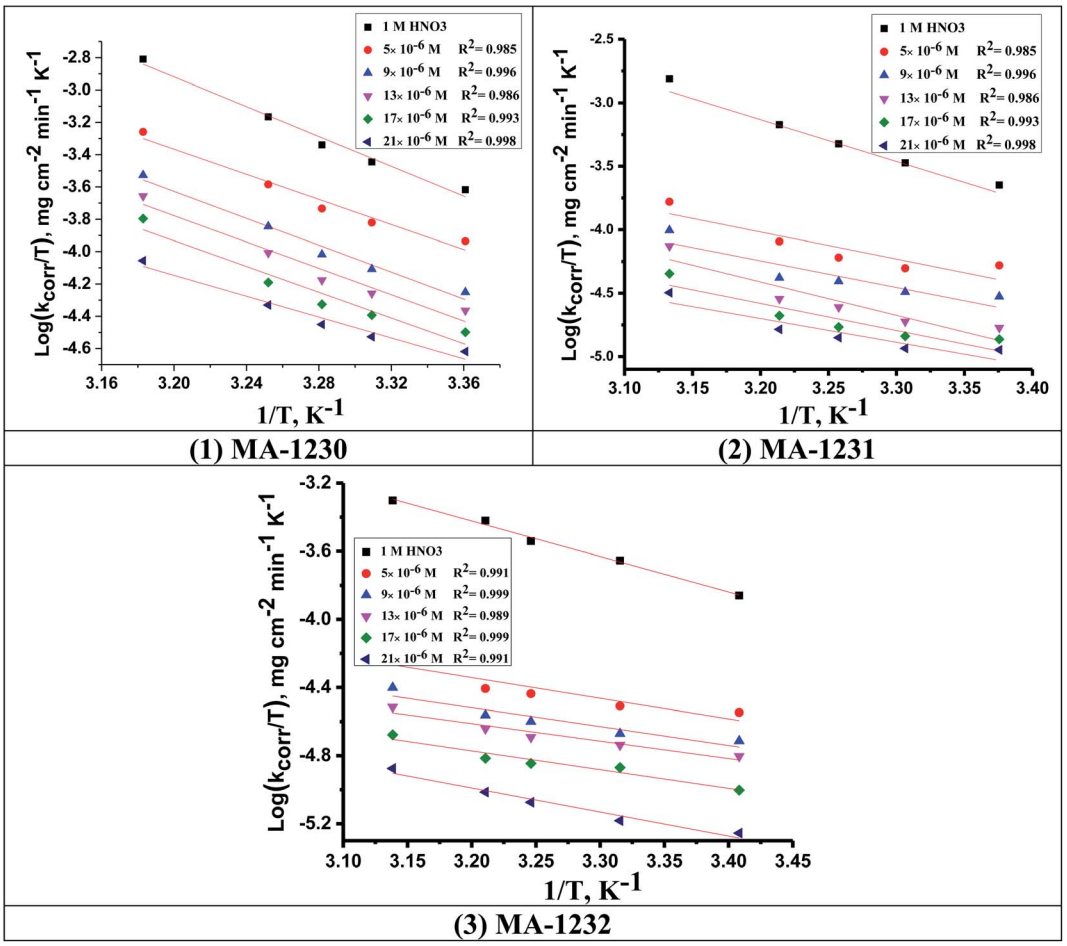

Fig. 3 Transition state plots (log k_{corr}/T *vs.* $1/T$) for Cu in 1 M HNO_3 in the absence and presence of different concentrations of (1) MA-1230, (2) MA-1231, and (3) MA-1232.

3.1.3. Adsorption study. The adsorption isotherm is an effective method for modeling the metallic surface adsorption activity of the investigated derivatives. The results were applied to a variety of adsorption isotherm models from WL experiments at different temperatures. It was noted that the Langmuir adsorption isotherm is the optimal one for testing the adsorption of the three derivatives of pyrimidine. The constant is given by eqn (4) (ref. 44)

Table 5 Thermodynamic adsorption parameters of MA-1230, MA-1231, MA-1232 adsorbed on the surface of the copper metal in 1 M HNO_3 acid at different temperatures

Inhibitor	Temp, °C	$-\Delta G^{\circ}_{ads}$, kJ mol^{-1}	ΔH°_{ads}, kJ mol^{-1}	ΔS°_{ads}, J mol^{-1} K^{-1}
MA-1230	25	42.7 ± 0.1732	30	24.4 ± 0.2028
	30	44.6 ± 0.2028		24.6 ± 0.2333
	35	44.9 ± 0.1453		24.3 ± 0.2028
	40	46.4 ± 0.2028		24.4 ± 0.1453
	45	51.2 ± 0.1764		25.5 ± 0.1453
MA-1231	25	44.5 ± 0.1732	149	65.1 ± 0.1732
	30	46.2 ± 0.2028		64.5 ± 0.1453
	35	48.4 ± 0.1732		64.2 ± 0.2028
	40	55.3 ± 0.1000		65.4 ± 0.1453
	45	55.7 ± 0.1453		64.5 ± 0.1732
MA-1232	25	44.5 ± 0.1732	135	60.2 ± 0.1764
	30	46.2 ± 0.2028		59.8 ± 0.1453
	35	48.4 ± 0.1732		59.5 ± 0.1732
	40	55.3 ± 0.1000		60.8 ± 0.2028
	45	55.7 ± 0.1453		60.1 ± 0.2309

$$\frac{C}{\theta} = \left(\frac{1}{K_{ads}}\right) + C \quad (4)$$

where K_{ads} is the adsorption equilibrium constant and C is the concentration of the derivatives in μM. The values of adsorption Gibbs free energy ΔG°_{ads} were calculated from eqn (5):

$$K_{ads} = \frac{1}{55.5} \exp\left(\frac{\Delta G^{\circ}_{ads}}{RT}\right) \quad (5)$$

Table 5 displays the negative values of the calculated ΔG°_{ads}, which indicate the spontaneity of the adsorption process.[45] When the ΔG°_{ads} values reached −55 kJ mol^{-1}, this indicated a highly chemical adsorption on the copper surface.[46,47] As a result of the value of ΔG°_{ads} and % η increasing with increasing temperature, the adsorption of these derivatives of pyrimidine often occurs through chemisorption. The heat of adsorption ΔH°_{ads} was calculated from the Van't Hoff equation:[48,49]

$$\ln K_{ads} = \frac{-\Delta H^{\circ}}{RT} + \text{constant} \quad (6)$$

Plots of log K_{ads} *vs.* $1/T$ for the tested derivatives of pyrimidine (Fig. 4) gave straight lines with slopes equal to $\Delta H^{\circ}_{ads}/2.303R$. We then calculated the value of the standard adsorption entropy ΔS°_{ads} from the thermodynamic basic eqn (7) (ref. 50–52) by introducing the values of ΔG°_{ads} and the values of ΔH°_{ads} at various temperatures:

$$\Delta G^{\circ}_{ads} = \Delta H^{\circ}_{ads} - T\Delta S^{\circ}_{ads} \quad (7)$$

3.2. Potentiodynamic polarization (PDP) measurements

Fig. 5 shows the PDP curves for the copper metal in 1 M HNO_3 solution with and without various concentrations of the tested derivatives (1–21 μM) at 25 °C. The cathodic and anodic curves shifted to lower values of the current density in the presence of the tested derivatives, thereby causing a decrease in the corrosion rate of Cu. The presence of these derivatives greatly reduced corrosion current density. A shift in the Tafel plot towards the cathodic region was observed. This indicated the repressive effect of these derivatives on the cathodic reaction. The differences in the profiles of anodic curves in the presence of these additives indicate the action of these additives on the anodic reaction. Therefore, these additives act as mixed inhibitors. The difference in the profile could be due to the formation of a barrier layer on the metal surface. Polarization parameters such as the corrosion current density (i_{corr}), (corrosion potential (E_{corr}) for blank and inhibited specimens at various concentrations, cathodic and anodic Tafel slopes (β_c & β_a), and the inhibition efficiency (η%)) for the pyrimidine derivatives are collected in Table 6. η% was calculated using the following relation:[53]

$$\%\ \eta_{PDP} = \left(\frac{i_{corr} - i'_{corr}}{i_{corr}}\right) \times 100 \quad (8)$$

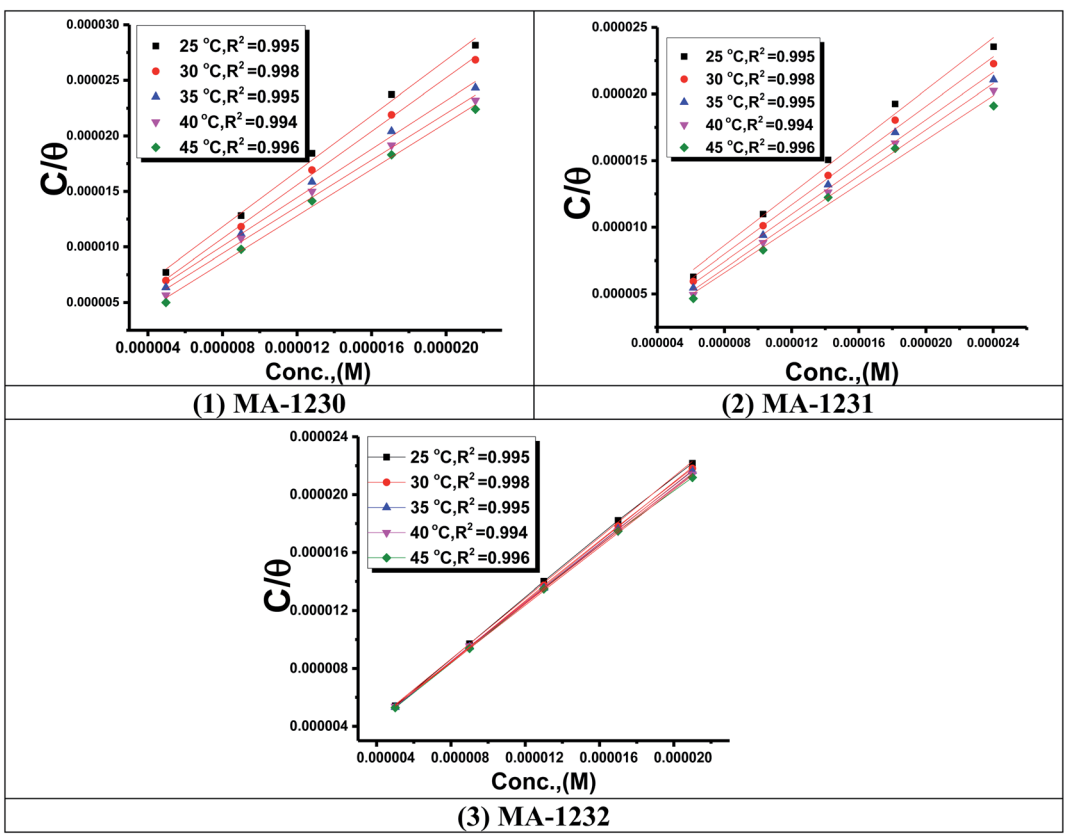

Fig. 4 Langmuir isotherm plots for the corrosion of copper in the 1 M HNO_3 with optimum concentrations of (1) MA-1230, (2) MA-1231, and (3) MA-1232 derivatives.

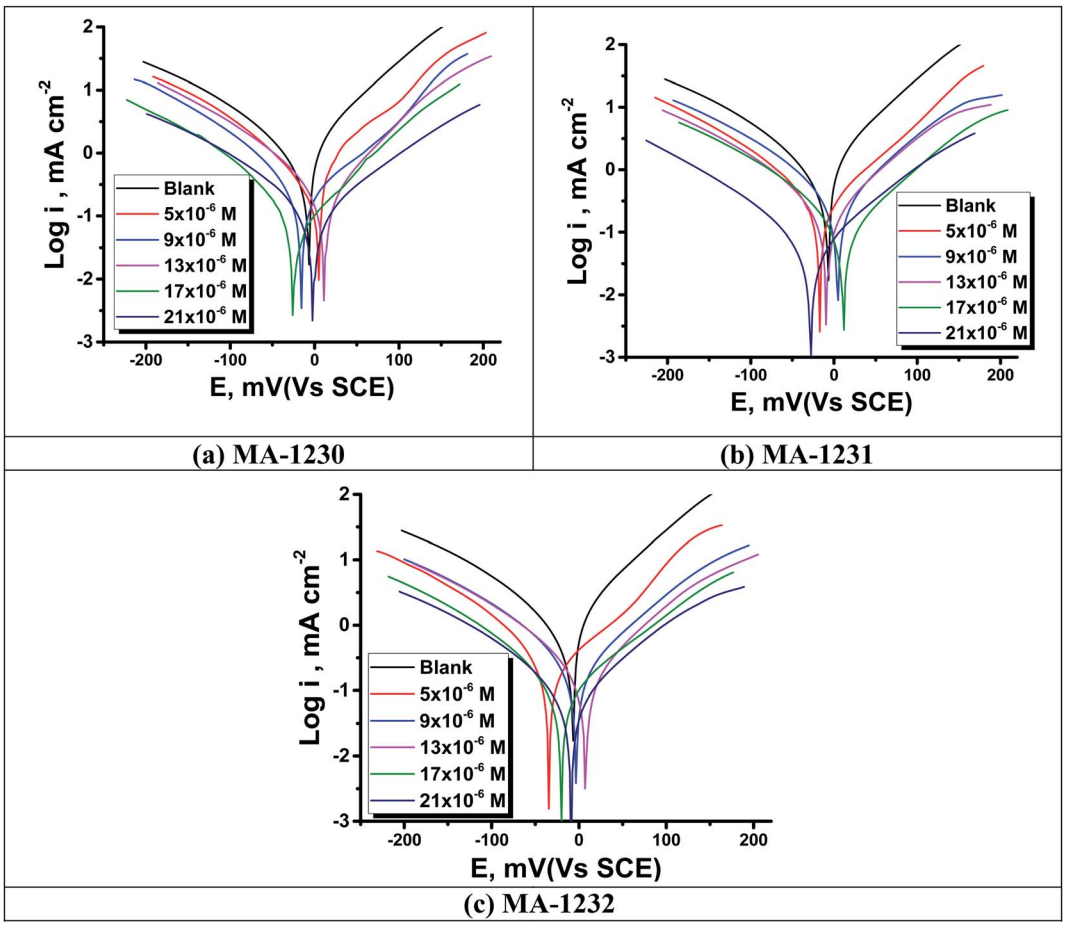

Fig. 5 PDP curves for Cu metal in the 1 M HNO_3 solution at different concentrations of derivatives (a) MA-1230, (b) MA-1231, and (c) MA-1232 at 25 °C.

where i'_{corr} and i_{corr} refer to the corrosion current densities of the copper metal with and without inhibitors, respectively. With decreasing (i_{corr}), the % η values increased as the inhibitor concentration increased as observed in Table 6.[54] The inhibitor can be anodic or cathodic if E_{corr} is greater than −85 mV per SCE as compared to the potential for the corrosion of the uninhibited blank, whereas the inhibitor can be considered as a mixed form if E_{corr} is less than −85 mV per SCE.[55] In our research, the shift was less than −27 mV per SCE, suggesting that the investigated derivatives are mixed type inhibitors.[56]

Table 6 PDP measurements for Cu metal in 1 M HNO_3 with and without various concentrations of the tested derivatives at 25 °C

Inhibitor	Conc., μM	$-E_{corr}$, mV *vs.* SCE	i_{corr}, μA cm^{-2}	β_a, mV dec^{-1}	$-\beta_c$, mV dec^{-1}	θ	% η
Blank	—	6.4 ± 0.2309	352.7 ± 0.1732	86.4 ± 0.2309	145.2 ± 0.2028	—	—
MA-1230	5	5.3 ± 0.2333	195.1 ± 0.1155	99.7 ± 0.2309	165.8 ± 0.3528	0.447	44.7
	9	15.5 ± 0.2028	153.6 ± 0.2028	102.9 ± 0.1453	126.9 ± 0.2028	0.565	56.5
	13	11.4 ± 0.1453	115.3 ± 0.2603	85.1 ± 0.1732	111.8 ± 0.1453	0.673	67.3
	17	26.4 ± 0.1453	81.6 ± 0.1764	88.7 ± 0.2309	98.0 ± 0.2906	0.769	76.9
	21	2.6 ± 0.1732	34.1 ± 0.2028	153.8 ± 0.2028	172.5 ± 0.1732	0.903	90.3
MA-1231	5	16.8 ± 0.1732	191.3 ± 0.1732	111.5 ± 0.2028	159.7 ± 0.1732	0.458	45.8
	9	5.1 ± 0.1453	149.6 ± 0.1764	127.1 ± 0.1732	157.3 ± 0.2028	0.576	57.6
	13	9.7 ± 0.1732	112.1 ± 0.1732	128.4 ± 0.1732	156.6 ± 0.17638	0.682	68.2
	17	12.7 ± 0.2082	73.2 ± 0.1732	118.8 ± 0.2309	142.2 ± 0.1732	0.792	79.2
	21	27.5 ± 0.2309	30.8 ± 0.2028	123.8 ± 0.1202	137.0 ± 0.2082	0.913	91.3
MA-1232	5	34.5 ± 0.2028	171.7 ± 0.1732	97.5 ± 0.2333	118.1 ± 0.1732	0.513	51.3
	9	3.2 ± 0.1732	139.2 ± 0.2309	121.7 ± 0.1453	183.8 ± 0.1155	0.605	60.5
	13	7.4 ± 0.1453	107.3 ± 0.1732	123.6 ± 0.20278	145.8 ± 0.2028	0.696	69.6
	17	20.3 ± 0.1453	64.1 ± 0.1453	157.9 ± 0.2603	166.9 ± 0.1764	0.818	81.8
	21	9.1 ± 0.2028	27.9 ± 0.1732	105.8 ± 0.2309	191.5 ± 0.2028	0.921	92.1

Fig. 6 An equivalent circuit model for measuring EIS data.

3.3. Electrochemical impedance spectroscopy (EIS) measurements

EIS studies afford details about the kinetics of the electrode processes and, concurrently, about the surface properties of the examined systems. Information can be derived from the shape of the impedance diagram.[57] The copper corrosion efficiency in the 1 M HNO_3 solution was examined by the EIS technique at 25 °C after 30 min of immersion in the presence and absence of various inhibitor concentrations. Fig. 6 shows an equivalent circuit used to consider all the processes involved in the electrical response of the system, which is a parallel combination of the charge-transfer resistance (R_{ct}) and the constant phase element (CPE), both in series with the solution resistance (R_s). The CPE element is used to explain the depression of the capacitance semi-circle, which corresponds to surface heterogeneity resulting from surface roughness impurities, dislocations, grain boundaries, adsorption of inhibitors, and the formation of porous layers.[58] The impedance of the CPE is represented by the following equation:

$$Z_{CPE} = 1/Y^{\circ}(j\omega)^{n} \quad (9)$$

where Y° represents the CPE constant, j is the imaginary root, ω is the angular frequency, n ($-1 < n < 1$) stands for the deviation index. The "n" values seem to be associated with the non-uniform distribution of current because of roughness and possible oxide surface defects. When $n = 1$, CPE is an ideal capacitor but true capacitive behavior is rarely obtained. The "n" values close to 1 (Table 7) represent the deviation from the ideal capacitor. A constant phase element (CPE) was utilized for data fitting instead of an ideal capacitor; since the "n" values obtained were in the range of 0.9, the value gained from the data fitting was taken as the capacitance. The quality of fitting to the equivalent circuit was assessed by the chi square value.[59] The obtained chi square values (0.000065 to 0.000123) in Table 7 indicate a good fitting to the proposed circuit. The Nyquist and Bode plots of the systems studied are indicated in Fig. 7 and 8, respectively. It is evident from Fig. 7 that Cu exhibited typical impedance behavior in 1 M HNO_3 solution for the investigated inhibitors examined and displayed a marked increase in the diameter for each concentration studied. The Nyquist graph of copper metal in 1 M HNO_3 solution deviated from the ideal circular shape because of the frequency dispersion.[60] It is worth noting that the changes in the concentration of the investigated inhibitors did not alter the profile of the impedance behavior, suggesting a similar mechanism for the corrosion inhibition of Cu by these inhibitors. This indicates that in the absence of inhibitors, the Nyquist plot for copper metal has a slightly depressed semicircular design, showing that in the 1 M HNO_3 solution, the charge transport mechanism mainly controls copper metal corrosion.[61] Fig. 8 represents two time constants; the first one appeared in the middle-frequency region and is related to the capacitive loop of the oxide layer on the Cu surface. The second time constant appeared in the low-frequency region and is attributed to the inductive loop arising from the relaxation process of the adsorbed inhibitor molecules on Cu surface or re-dissolution of the Cu oxide layer surface.[62] On adding the investigated inhibitors to the solution, the diameter of the semi-circle increased and retarded the corrosion of Cu by increasing the polarization resistance, R_p and decreasing the CPE values. Thus, the effectiveness of the investigated compounds was associated with higher values of R_p and low CPE values. This increase became more obvious as the inhibitor concentration increased, suggesting the adsorption of inhibitors on the copper specimen surface.[63] Bode diagrams illustrated the same behavior. From the Bode plots, a characteristic with one time constant was observed, corresponding to

Table 7 EIS parameter measurements for copper metal in 1 M HNO_3 with and without different concentrations of additives at 25 °C

Conc, μM		R_s, Ω cm^2	Y° (CPE), μΩ^{-1} s^n cm^{-2}	N	C_{dl}, μF cm^{-2}	R_{ct}, Ω cm^2	% η_{EIS}	χ^2
Blank		1.839	576.2	0.983	316.2 ± 0.2333	68.2 ± 0.1453	—	0.000087
MA-1230	5	2.117	427.3	0.969	193.1 ± 0.1453	134.5 ± 0.1764	49.32	0.000341
	9	2.238	381.6	0.985	171.4 ± 0.17634	176.1 ± 0.2028	61.29	0.000653
	13	2.291	332.1	0.951	127.9 ± 0.1453	245.3 ± 0.2028	72.21	0.000453
	17	2.418	291.2	0.985	91.3 ± 0.1732	387.2 ± 0.2309	82.40	0.000654
	21	2.782	250.9	0.871	63.2 ± 0.1732	805.7 ± 0.1732	91.54	0.000745
MA-1231	5	1.941	418.5	0.928	188.3 ± 0.1453	139.4 ± 0.2028	51.10	0.000065
	9	1.987	378.1	0.985	167.2 ± 0.2333	181.1 ± 0.1732	62.36	0.000451
	13	2.169	324.6	0.963	124.6 ± 0.1453	254.3 ± 0.2028	73.20	0.000123
	17	2.397	285.7	0.995	87.5 ± 0.1000	412.9 ± 0.1732	83.49	0.000231
	21	2.489	231.4	0.926	58.4 ± 0.1202	859.6 ± 0.1732	92.07	0.000129
MA-1232	5	1.147	406.2	0964	173.9 ± 0.1732	157.9 ± 0.1453	56.83	0.000238
	9	1.976	371.5	0.9931	162.5 ± 0.1732	184.1 ± 0.2028	62.98	0.000454
	13	2.081	319.1	0.985	119.2 ± 0.2309	267.4 ± 0.1732	74.51	0.000462
	17	2.673	274.6	0.913	75.4 ± 0.2028	491.5 ± 0.1732	86.13	0.000653
	21	2.927	211.9	0.895	47.1 ± 0.2028	1016.2 ± 0.1732	93.29	0.000762

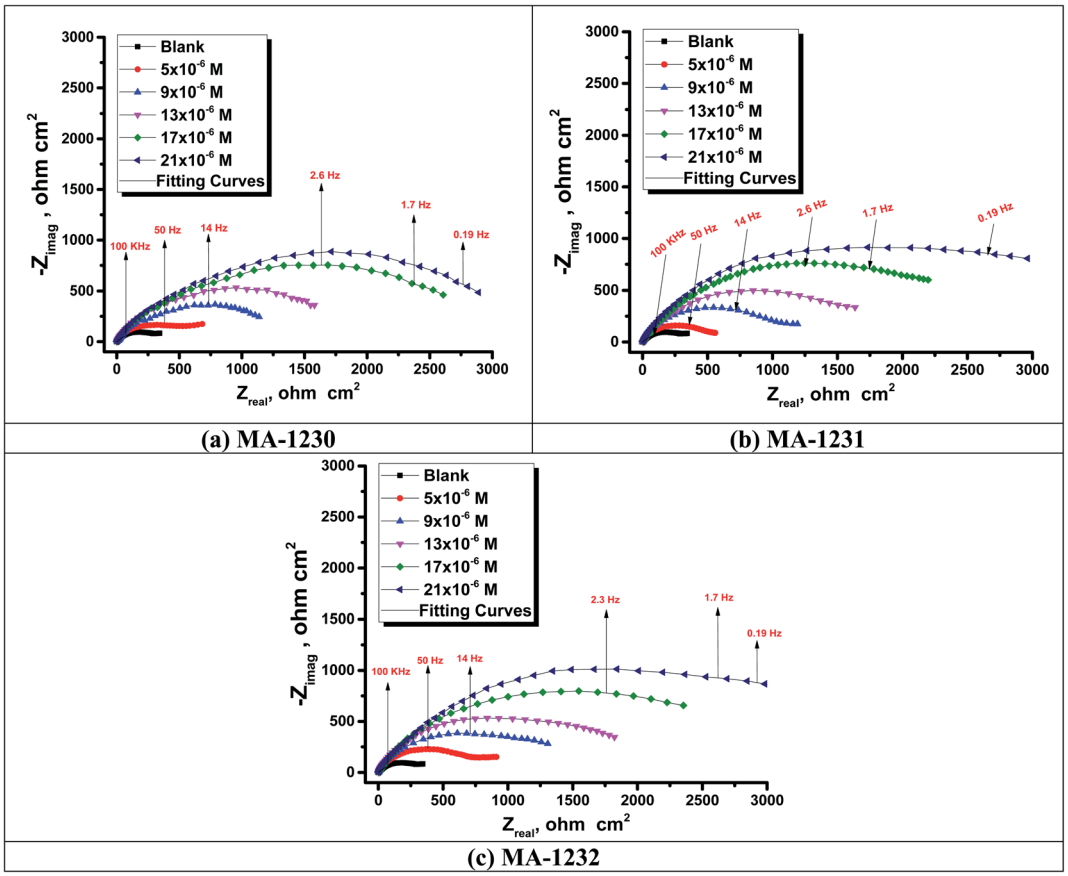

Fig. 7 Nyquist plots for copper metal in 1.0 M HNO_3 without and with different concentrations of (a) MA-1230, (b) MA-1231, and (c) MA-1232 at 25 °C.

the capacitance loop. These results suggest that Cu has better corrosion resistance in the presence of these derivatives. In Table 7, the various impedance parameters, namely, charge transfer resistance (R_{ct}), double layer capacitance (C_{dl}), Y° (CPE), n, goodness of fit χ^2 and % η_{EIS} are cited. The CPE and their n values represent double-layer capacitors with some holes.[64] The decrease in Y° (CPE) values with increasing concentration of inhibitors resulted from a decrease in the local dielectric constant and/or an increase in the thickness of the double layer, suggested that these inhibitor molecules inhibited the Cu corrosion by adsorption at the Cu/HNO_3 interface. The increase in the R_{ct} values with increasing inhibitor concentration was always greater as compared to in its absence, which indicates that these additives are adsorbed on the Cu surface, forming a protective layer. This layer performs as a barrier for mass and charge transfer.[65] The R_{ct} values reached the maximum value at 21 μM for all additives, which indicates the decrease in the corrosion rate. On the other hand, the C_{dl} values decreased on raising the concentration of additives due to the increase in the inhibitor concentration.[66]

The C_{dl} value was obtained from the following equation:[67]

$$C_{dl} = \frac{1}{2\pi f_{max} R_{ct}} \quad (10)$$

The corrosion % η was calculated by using the following equation:

$$\%\ \eta_{EIS} = \left(\frac{R_{ct} - R_{ct}^{*}}{R_{ct}}\right)$$

11where R_{ct}^{*} is the charge transfer resistance without the inhibitor, R_{ct} is the charge transfer resistance with the inhibitor. η% increases due to the formation of an adsorbed layer from additives on the copper surface, and this layer increases in thickness by increasing the concentration of the additives.[68] The EIS research also gave approximately the same efficiency of inhibition as obtained in WL and PDP measurements.

3.4. Surface analysis

3.4.1. Scanning electron microscope (SEM) analysis. The morphology of the copper metal surface was investigated by scanning electron microscopy when the copper samples were immersed in 1 M HNO_3 solution for 24 with and without the tested inhibitors. Fig. 9a represents the freshly abraded copper sample before immersion, showing a smooth surface, while Fig. 9b shows the image of the Cu sample dipped in HNO_3 for 24 h, where the surface of Cu was corroded due to the aggressive attack of the acid solution. In the presence of pyrimidine inhibitors with a 21 μM concentration, the surfaces of the Cu samples became smoother, as shown in Fig. 9c–e.[69] The presence of pyrimidine derivatives as

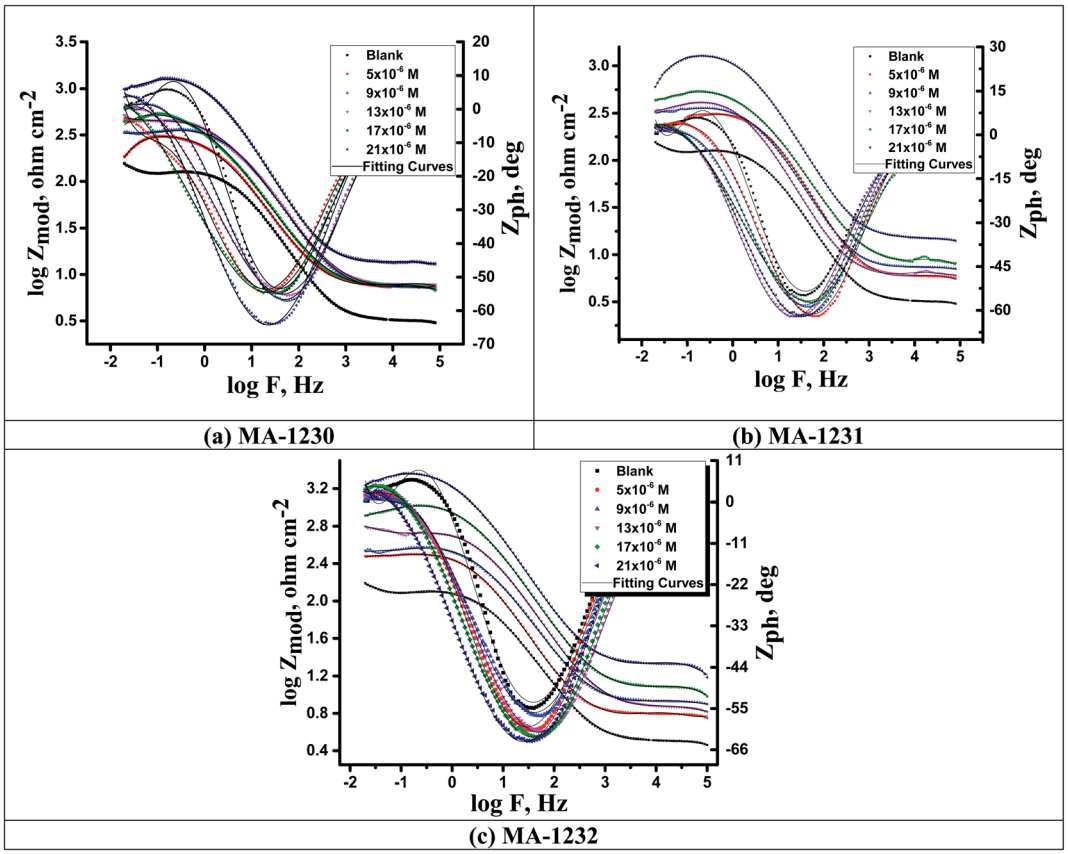

Fig. 8 Bode plots for copper metal in 1 M HNO_3 without and with different concentrations of (a) MA-1230, (b) MA-1231, and (c) MA-1232 at 25 °C.

a corrosion inhibitor in the corrosive medium leads to a relatively cleaner surface. This also implies a greater ability for corrosion inhibition by pyrimidine molecules. The morphology of the copper metal samples was smoother in the following order: MA-1232 > MA-1231> MA-1230. From the results, one can conclude that a protective film was formed by the used inhibitor molecules on the Cu surface, which led to the significant inhibition of the corrosion of Cu in acid medium.

3.4.2. Energy dispersive X-ray (EDX) analysis. Energy Dispersive X-ray Analysis (EDX) is a technique used to get information on the composition of the corrosion substance on the copper metal surface in the absence and presence of the highest concentration of inhibitor when immersed in a 1 M HNO_3 solution. Fig. 10a shows that the polished surface of the copper metal has a large copper peak and shows great surface properties, whereas after immersing in 1 M HNO_3 without the inhibitors (Fig. 10b), there was great damage to the copper sample due to the strong corrosion; the iron peak strength was increased in the presence of the inhibitor, which indicates the coverage of the copper surface with the inhibitor molecules, as shown in Fig. 10c–e.[70] By adding 21×10^{-6} M of inhibitors, the enhancement of the copper metal surface was observed due to the strong protective film of the inhibitor molecules on the surface of the copper sample; a decrease in the iron band was observed, as indicated in Fig. 10c–e. The protective layer produced by inhibitor molecules was strongly surface adherent, which leads to evidence of efficient inhibition performance.[71]

3.5. Quantum calculations

The gap in the energy band ($\Delta E = E_{LUMO} - E_{HOMO}$), which is the energy required to eliminate an electron from the last orbital occupied, may influence the efficiency of inhibition and small absolute energy band gap values would have strong inhibition efficiencies.[72] The dipole moment (μ) is a measure of the polarity of the covalent bond between the compounds studied. It is accepted that high μ values improve the adsorption tendency on the metal surfaces of the compounds tested. The order of ΔE values in theoretical calculations of band gap energy is as follows: MA-1230 > MA-1231 > MA-1232. The decreasing inhibition efficiency order showed a good correlation with corrosion efficiency. All results in Fig. 11 and Table 8 illustrate the lowest total energy in the inhibitor MA-1232 (1,3-diethyl-2-thiobarbituric acid-bithiophene scaffold), which means that the adsorption of the inhibitor MA-1232 is highest, with the highest softness. The global hardness (η), softness (σ), and chemical potential (μ) were calculated in terms of I_P and E_A73 from the following equations:

$$\mu = -\chi = -\frac{I_p + E_A}{2} \quad (11)$$

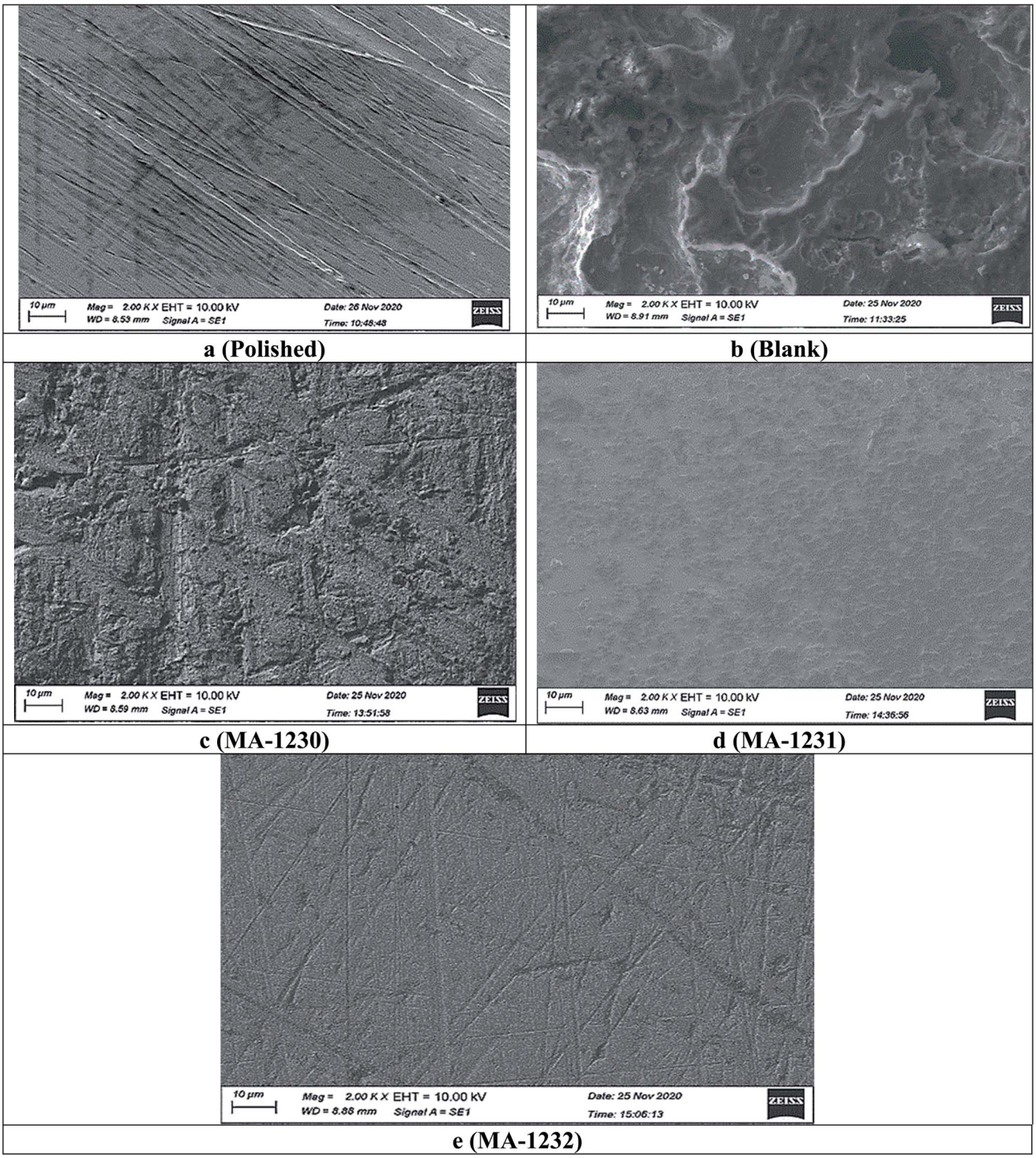

Fig. 9 SEM micrographs of copper metal without (blank) and with 21 μM of the tested derivatives (a–e).

$$\chi = \frac{I_p + E_A}{2} \quad (12)$$

$$\eta = \frac{I_p - E_A}{2} \quad (13)$$

$$\sigma = \frac{1}{\eta} \quad (14)$$

The above results reveal that the heteroatoms (N, O, and S) in inhibitor molecule structures have a great influence on the quantum chemical parameters. This theoretically demonstrates that the heteroatom (S) could cause effects on the adsorption of the inhibitor molecules on the metal. We performed further molecular dynamics calculations on the adsorption of the inhibitors on the copper surface as outlined in the following.

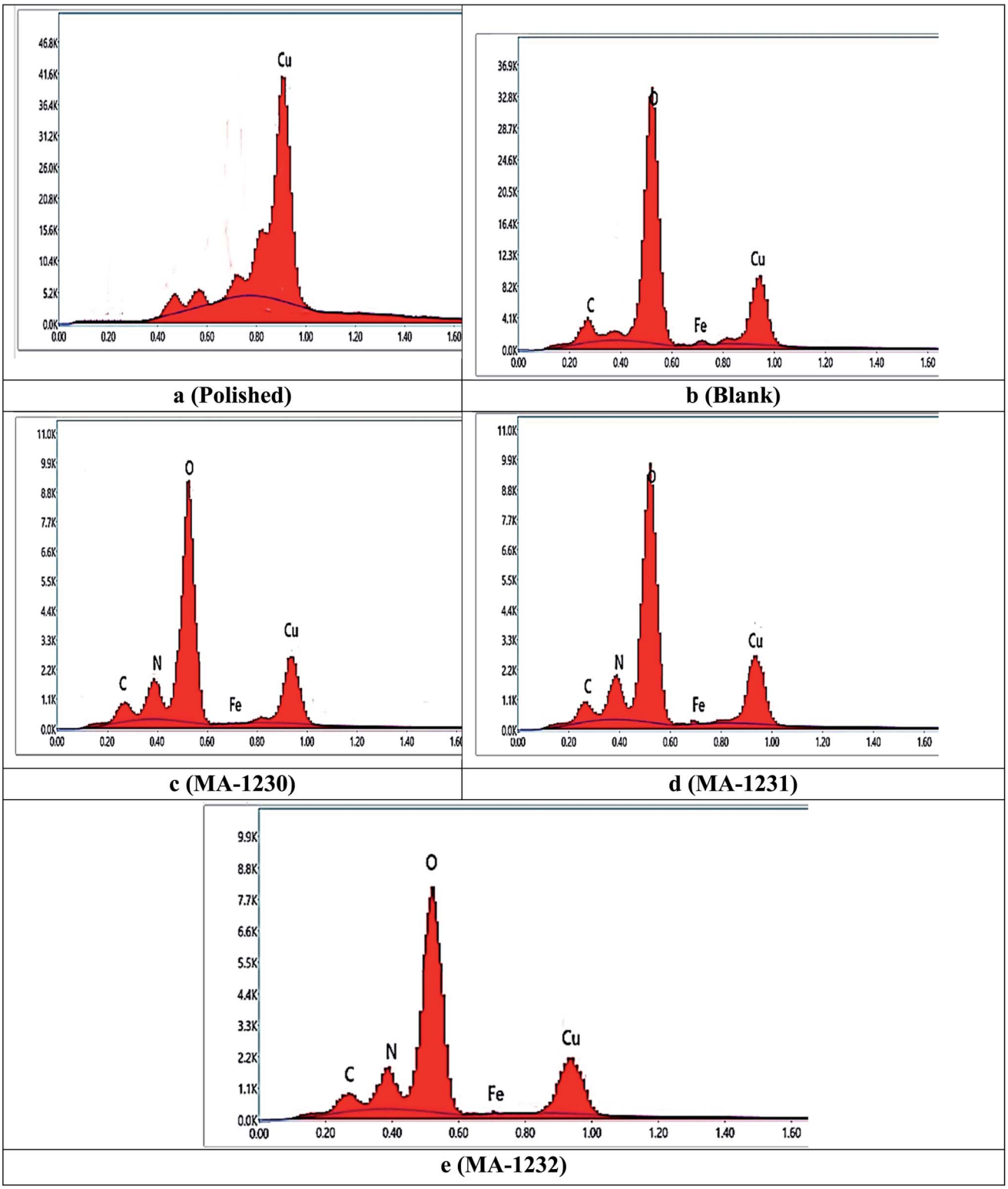

Fig. 10 EDX micrographs of copper metal without (blank) and with 21 × 10^{-6} M of the investigated derivatives (a–e).

3.6. Monte Carlo (MC) simulation

MC simulation is a perfect simulation tool for finding the most stable adsorption conformations in 1 M HNO_3 of the substituted pyrimidine-bichalcophene derivatives. The results of the simulations of the investigated derivatives are shown in Fig. 12 and are listed in Table 9. Fig. 12 shows the most favorable configuration of the adsorbed molecules on the metal surface of Cu (110). The molecules mentioned are adsorbed on the surface of the metal from the motive, which is rich in electrons from these inhibitory molecules. The established

interactions between the occupied orbitals of the investigated derivatives and the unoccupied orbitals of Cu (110) are expressed by the values of adsorption energy (E_{ads}), rigid energy (E_{rigid}), deformation energy (E_{def}), and energy ratios (dE_{ads}/E_{Ni}) of the inhibitors; these values are collected in Table 9. The results indicate that these inhibitory structures behave as active voltages. Adsorption energy is characterized as declining energy when two materials are mixed during the adsorption process in which an electron, ion, or molecule (adsorbent) is bound to the solid surface.[74] As seen in Table 8, the order of higher energy of relative adsorption is MA-1232 > MA-1231 > MA-1230, which predicts the heavy adsorption of MA-1232 (1,3-diethyl-2-thiobarbituric acid-bithiophene scaffold) on the hardened copper surface creating a stable adsorbed layer that protects the copper from dissolution. These derivatives protect the Cu studied in HCl medium from corrosion. This is in keeping with experimental studies.

4. Mechanism of corrosion hindrance

Adsorption can be demonstrated by physicochemical characteristics (*e.g.* types of electron density, functional groups) and the Cu charge, based on experimental studies and theoretical calculations. Fig. 13 shows the possible inhibition mechanism of these pyrimidine derivatives on the surface of Cu. Several studies have indicated that the Cu surface in HNO_3 solution is positively charged, *i.e.*, on the Cu surface, there are several positive charges.[75] The positively charged Cu surface prefers NO^{3-} adsorption to create a negatively charged surface, which makes it easier to adsorb the cations in the solution. These organic pyrimidine-bichalcophenes can be protonated in the solution because of the unshared electron pairs of the N, O and S electrons. Electrostatic interactions lead to the adsorption of protonated molecules on the specimen surface, *i.e.*,

Table 8 Quantum chemical parameters for the studied organic inhibitors

Compound	MA-1230	MA-1231	MA-1232
E_{HOMO}, eV	−10.1	−9.28	−8.97
E_{LUMO}, eV	−1.62	−1.71	−1.96
ΔE, eV	8.48	7.57	7.01
I_P, eV	10.1	9.28	8.97
E_A, eV	1.62	1.71	1.96
η, eV	4.240	3.785	3.505
σ, eV	0.236	0.264	0.285
μ, eV	5.860	5.495	5.465
Dipole moment (debye)	2.790	3.170	4.300

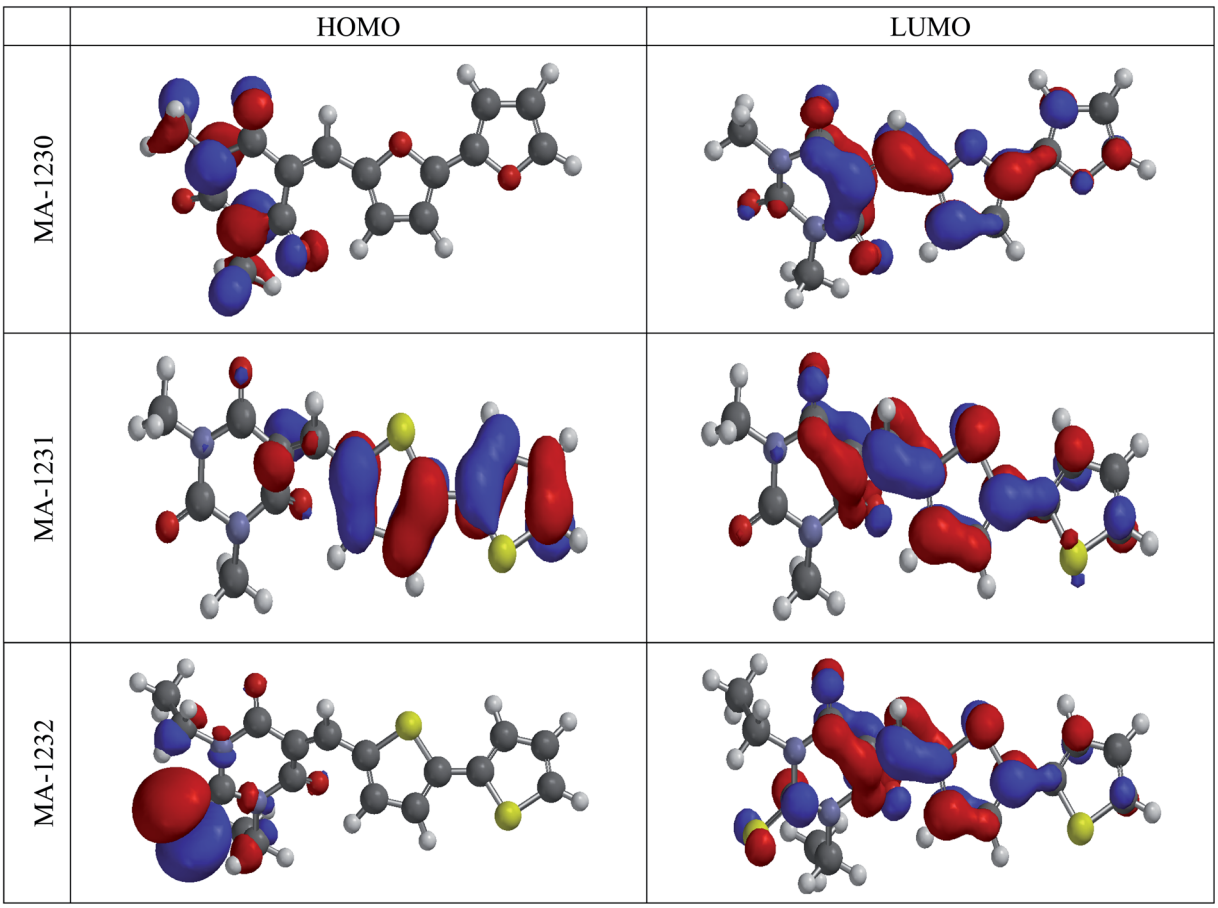

Fig. 11 The frontier molecular orbital provides the electron density maps of HOMO and LUMO for the tested inhibitors.

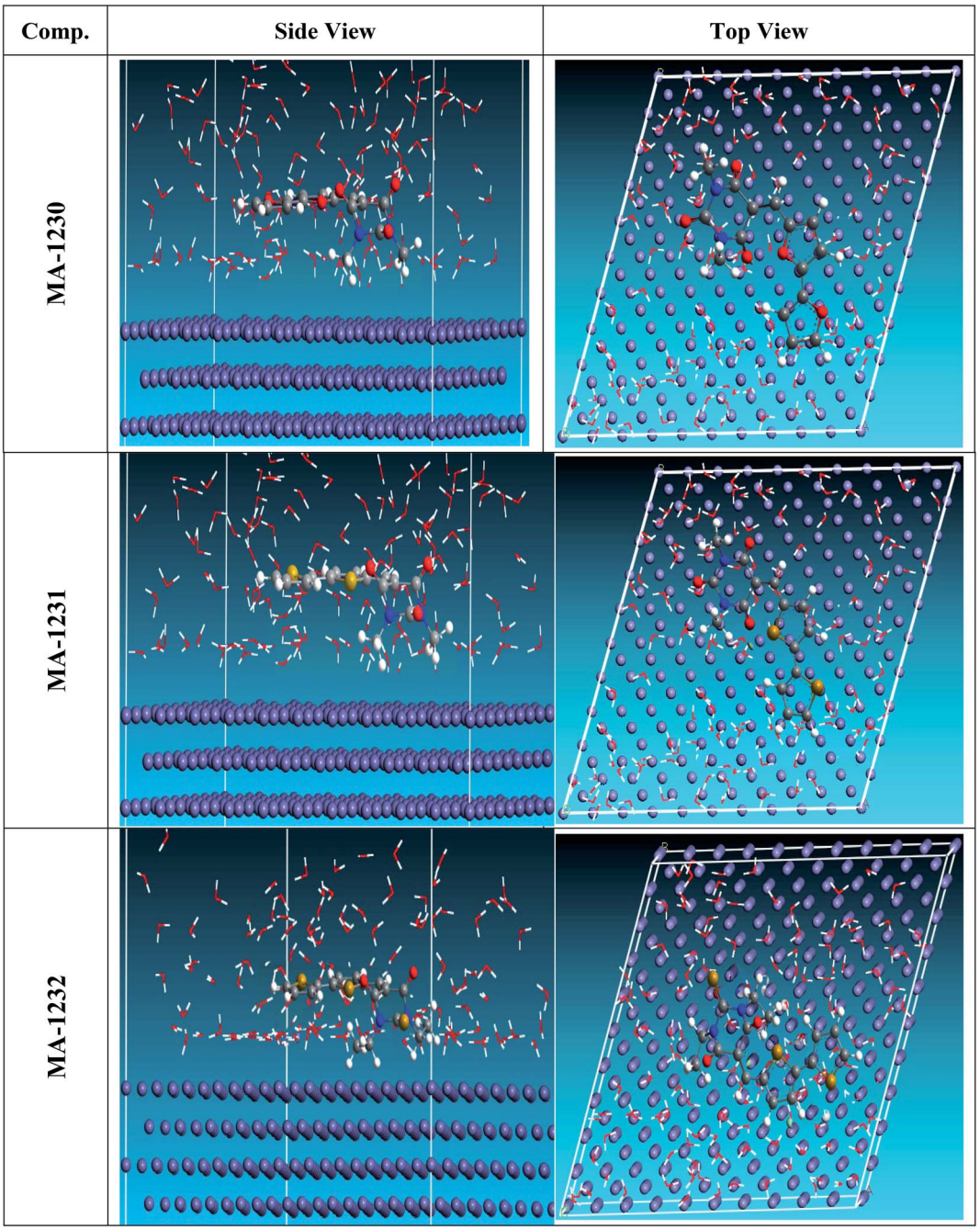

Fig. 12 The most suitable configuration for the adsorption of the organic molecules on the Cu (1 0 0) substrate obtained by the adsorption locator module.

physisorption. Meanwhile, by forming covalent bonds (chemisorption), further adsorption of these inhibitor molecules could be realized, as shown in Fig. 13. Quantum chemical measurements of both WL and electrochemical values indicated the % IE of the three investigated pyrimidine-bichalcophene derivatives as follows: MA-1232 > MA-1231 >

Table 9 Data and descriptors calculated by the Monte Carlo simulation for the adsorption of compound molecules on copper (1 0 0)

Structures	Total energy	Adsorption energy	Rigid adsorption energy	Deformatio energy	Compound dE_{ad}/dNi	H_2O dE_{ad}/dNi
Cu (1 0 0)/MA-1232/H_2O	−3211.16	−4108.929	−4039.791	−69.138	−263.097	−12.522
Cu (1 0 0)/MA-1231/H_2O	−3205.42	−4103.314	−4034.503	−68.811	−278.272	−8.06
Cu (1 0 0)/MA-1230/H_2O	−3198.75	4099.094	−4029.213	69.881	−288.447	−6.926

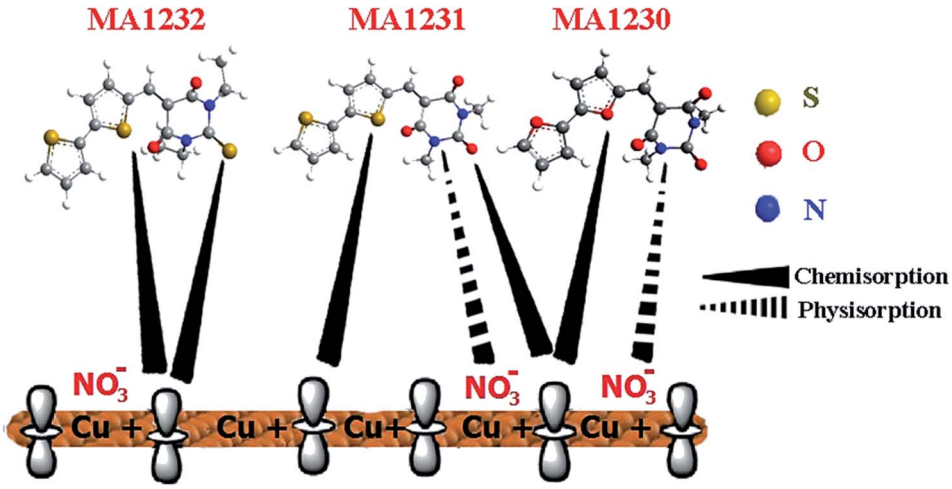

Fig. 13 A schematic diagram of the corrosion protection of Cu dipped in 1 M HNO_3 corrosion medium with pyrimidine derivatives (MA-1232, MA-1231, and MA-1230).

MA-1230. MA-1232 is the most efficient inhibitor because it contains 3 S, 2 N and 2 O atoms, 2 ethyl groups as substituents and has the highest molecular size, which covers more surface area; however, MA-1231 contains 2 S, 2 N, 2 O atoms, 2 methyl groups as substituents and has a smaller molecular size than MA-1232 (ethyl groups are more efficient than methyl groups). MA-1230 is the least efficient at inhibition due to its containing 2 N and 5 O atoms (S > N > O in basicity) and it has the smallest molecular size.

5. Conclusions

Pyrimidine-bichalcophene derivatives (MA-1232, MA-1231, and MA-1230) were studied as inhibitors in 1 M HNO_3 for Cu corrosion. The data gained from chemical tests (WL) and electrochemical (PDP, and EIS) procedures revealed that the protection was dependent on the dose of the pyrimidine-bichalcophenes and the temperature. The investigated pyrimidine-bichalcophenes predominantly acted as mixed inhibitors on the copper in 1 M $HNO_3$and the adsorption was described by the Langmuir adsorption isotherm. C_{dl} diminished while R_{ct} increased with increasing the doses of the tested inhibitors, which can be attributed to the adsorbed inhibitor molecules. Pyrimidine-bichalcophene molecules established a protective layer over the copper surface. There was strong agreement between the chemical and electrochemical techniques. A comparative study of pyrimidine-bichalcophene derivatives (MA-1232, MA-1231, and MA-1230) using quantum chemical study confirmed the experimental results. The results obtained by MC simulation showed that the binding performance between the products used and the metal surface of Cu (110) was in the following order: $E_{binding}$ MA-1232 > $E_{binding}$ MA-1231 > $E_{binding}$ MA-1230.

Conflicts of interest

The authors declare that there is no conflict of interest between them and anybody else.

References

1 P. R. Roberge, *Handbook of corrosion engineering*, New York, McGraw-Hill, 2000.
2 S. S. Abdel-Rehim, K. F. Khaled and N. S. Abd-Elshafi, *Electrochim. Acta*, 2019, **51**, 3269.
3 R. Touir, R. A. Belakhmima, M. E. Touhami, L. Lakhrissi, M. El Fayed, B. Lakhrissi and E. M. Essassi, Comparative inhibition study of mild steel corrosion in hydrochloric acid by benzimidazole derivatives, *J. Mater. Environ. Sci.*, 2013, **4**, 921–930.
4 A. M. El Defrawy, M. Abdallah and J. H. Al-Fahemi, Electrochemical and theoretical investigation for some pyrazolone derivatives as inhibitors for the corrosion of C-steel in 0.5 M hydrochloric acid, *J. Mol. Liq.*, 2019, **288**, 110994.
5 A. S. Fouda, M. A. Ismail, A. S. Abousalem and G. Y. EL-Elewady, Experimental and theoretical studies on corrosion inhibition of 4-amidinophenyl-2,2′-bifuran and its analogues in acidic solutions, *RSC Adv.*, 2017, **7**, 46414–46430.
6 J. Patoczka and G. W. Pulliam, Biodegradation, and secondary effluent toxicity of ethoxylated surfactants, *Water Resour.*, 1990, **24**, 965–972.
7 N. Fatma, M. Panda and W. H. Ansari, Environment-friendly ester bonded gemini surfactant: mixed micellization of 14-E2-14 with ionic and nonionic conventional surfactants, *J. Mol. Liq.*, 2015, **211**, 247–255.
8 N. N. Al-Mohammed, R. S. D. Hussen, Y. Alias and Z. Abdullah, Tris-imidazolium and benzimidazolium ionic liquids: a new class of biodegradable surfactants, *RSC Adv.*, 2015, **5**, 2869–2881.
9 T. Tatsumi, W. Zhang, T. Kida, Y. Nakatsuji, D. Ono, T. Takeda and I. Ikeda, Novel hydrolyzable and biodegradable cationic gemini surfactants: bis(ester-ammonium) dichloride having a butenylene or a butynylene spacer, *J. Surfactants Deterg.*, 2001, **4**, 279–285.

10 T. Zhou, J. Yuan, Z. Zhang, X. Xin and G. Xu, The comparison of imidazolium Gemini surfactant [C_{14}-4-C_{14}im] Br_2 and its corresponding monomer as corrosion inhibitors for A3 carbon steel in hydrochloric acid solutions: experimental and quantum chemical studies, *Colloids Surf., A*, 2019, **575**, 57–65.

11 A. S. Fouda, N. Nawar, M. A. Ismail, A. A. Zaher and A. S. Abousalem, The inhibition action of methoxy-substituted phenylthienylbenzamidines on the corrosion of carbon steel in hydrochloric acid medium, *J. Mol. Liq.*, 2020, **312**, 113267.

12 A. S. Abousalem, M. A. Ismail and A. S. Fouda, A complementary experimental and in silico studies on the action of fluorophenyl 2,2′ bichalcophenes as ecofriendly corrosion inhibitors and biocide agents, *J. Mol. Liq.*, 2019, **276**, 255–274.

13 A. S. Fouda, M. A. Ismail, A. A. Al-Khamri and A. S. Abousalem, Experimental, quantum chemical and molecular simulation studies on the action of arylthiophene derivatives as acid corrosion inhibitors, *J. Mol. Liq.*, 2019, **290**, 111178.

14 M. A. Ismail, R. K. Arafa, M. M. Youssef and W. M. El-Sayed, Anticancer, antioxidant activities, and DNA affinity of novel monocationic bithiophenes and analogues, *Drug Des., Dev. Ther.*, 2014, **8**, 1659–1672.

15 W. A. Hussin, M. A. Ismail, A. M. Alzahrani and W. M. El-Sayed, Evaluation of the biological activity of novel monocationic fluoroaryl-2,2′-bichalcophenes and their analogues, *Drug Des., Dev. Ther.*, 2014, **8**, 963–972.

16 M. M. Youssef, M. A. Al-Omair and M. A. Ismail, Synthesis, DNA affinity, and antimicrobial activity of 4-substituted phenyl-2,2′-bichalcophenes and aza-analogues, *Med. Chem. Res.*, 2012, **21**, 4074–4082.

17 K. Rasheeda, V. D. P. Alva, P. A. Krishnaprasad and S. Samshuddin, Pyrimidine derivatives as potential corrosion inhibitors for steel in acid medium – an overview, *Int. J. Corros. Scale Inhib.*, 2018, **7**, 48–61.

18 K. R. Ansari, A. S. Sudheer and M. A. Quraishi, Some Pyrimidine Derivatives as Corrosion Inhibitor for Mild Steel in Hydrochloric Acid, *J. Dispersion Sci. Technol.*, 2015, **36**, 908–917.

19 K. R. Ansari, Sudheer, A. Singh and M. A. Quraishi, Some pyrimidine derivatives as corrosion inhibitor for mild steel in hydrochloric acid, *J. Dispersion Sci. Technol.*, 2015, **36**, 908–917.

20 H. Ashassi-Sorkhabi, B. Shaabani and D. Seifzadeh, Effect of some pyrimidinic Schiff bases on the corrosion of mild steel in hydrochloric acid solution, *Electrochim. Acta*, 2005, **50**, 3446–3452.

21 M. Yadav, S. Kumar, R. R. Sinha, I. Bahadur and E. E. Ebenso, New pyrimidine derivatives as efficient organic inhibitors on mild steel corrosion in acidic medium: electrochemical, SEM, EDX, AFM and DFT studies, *J. Mol. Liq.*, 2015, **211**, 135–145.

22 S. Lahmidi, A. Elyoussfi, A. Dafali, H. Elmsellem, N. K. Sebbar, L. El Ouasif, A. E. Jilalat, B. El Mahi, E. M. Essassi, I. Abdel-Rahman and B. Hammouti, Corrosion inhibition of mild steel by two new 1,2,4-triazolo [1,5-a]pyrimidine derivatives in 1 M HCl: experimental and computational study, *J. Mater. Environ. Sci.*, 2017, **8**, 225–237.

23 C. Verma, M. A. Quraishi, K. Kluza, M. M. Janusik, L. O. Olasunkanmi and E. E. Ebenso, Corrosion inhibition of mild steel in 1 M HCl by D-glucose derivatives of dihydropyrido[2,3-d:6,5-d′]dipyrimidine-2,4,6,8(1H,3H,5H,7H)-tetraone, *Sci. Rep.*, 2017, **7**, 44432.

24 P. B. Shetty, T. H. S. Kumara, D. M. Mamatha, V. R. Rao and A. C. Hegde, Inhibition effect of a new pyrimidine derivative on the corrosion of mild steel in hydrochloric acid solution, *Surf. Eng. Appl. Electrochem.*, 2017, **53**, 42–51.

25 A. Yurt, A. Balaban, S. U. Kandemir, G. Bereket and B. Erk, Investigation on some Schiff bases as HCl corrosion inhibitors for carbon steel, *Mater. Chem. Phys.*, 2004, **85**, 420–426.

26 M. A. Ismail, An efficient synthesis of 5′-(4-cyanophenyl)-2,2′-bifuran-5-carbonitrile and analogues, *J. Chem. Res.*, 2006, **11**, 733–737.

27 X. Su, H. Zhang, K. You, H. Wang, Y. Cui and W. W. Yu, Barbituric Derivative Nanoaggregates with Aggregation-Induced Emission and Mechanofluorochromism, *J. Nanomater.*, 2019, **2019**, 1–10, DOI: 10.1155/2019/7635756.

28 X. Luo, X. Pan, S. Yuan, S. Du, C. Zhang and Y. Liu, Corrosion inhibition of mild steel in simulated seawater solution by a green eco-friendly mixture of glucomannan (GL) and bisquaternary ammonium salt (BQAS), *Corros. Sci.*, 2017, **125**, 139–151.

29 A. S. Fouda, M. A. Abd El-Ghaffar, M. H. Sherif, A. Taher El-Habab and A. El-Hossiany, *Prot. Met. Phys. Chem. Surf.*, 2020, **56**, 89–201.

30 K. Ansari and M. Quraishi, Experimental and quantum chemical evaluation of Schiff bases of isatin as a new and green corrosion inhibitor for mild steel in 20% H_2SO_4, *J. Taiwan Inst. Chem. Eng.*, 201, **54**, 145–154.

31 B. Qian, J. Wang, M. Zheng and B. Hou, Synergistic effect of polyaspartic acid and iodide ion on corrosion inhibition of mild steel in H_2SO_4, *Corros. Sci.*, 2013, **75**, 184–192.

32 B. M. Hussein, M. A. Migahed, M. M. Shaban, N. A. Negm and Z. Moawad, Synthesis and Inhibition Performance of Diquaternary Ammonium Gemini Surfactants on Carbon Steel Pipelines Corrosion in Gas Field, in *Offshore Mediterr. Conf. Exhib., Offshore Mediterranean Conference*, pp. OMC-2017, 731.

33 F. F. Eliyan, E. S. Mahdi and A. Alfantazi, Electrochemical evaluation of the corrosion behavior of API-X100 pipeline steel in aerated bicarbonate solutions, *Corros. Sci.*, 2012, **58**, 181–191.

34 V. D. Jović and B. M. Jović, EIS and differential capacitance measurements onto single crystal faces in different solutions: part I: Ag (111) in 0.01 M NaCl, *J. Electroanal. Chem.*, 2003, **541**, 1–11.

35 H. Ashassi-Sorkhabi, N. Ghalebsaz-Jeddi, F. Hashemzadeh and H. Jahani, Corrosion inhibition of carbon steel in hydrochloric acid by some polyethylene glycols, *Electrochim. Acta*, 2006, **51**, 3848–3854.

36 R. S. Gonçalves, D. S. Azambuja and A. M. S. Lucho, Electrochemical studies of propargyl alcohol as corrosion inhibitor for nickel, copper, and copper/nickel (55/45) alloy, *Corros. Sci.*, 2007, **44**, 467–479.

37 M. M. Shaban, A. M. Eid, R. K. Farag, N. A. Negm, A. A. Fadda and M. A. Migahed, Novel trimeric cationic pyrdinium surfactants as bi-functional corrosion inhibitors and antiscalants for API 5L X70 carbon steel against oilfield formation water, *J. Mol. Liq.*, 2020, **305**, 112817.

38 J. R. Macdonald and W. B. Johanson, in *Theory in Impedance Spectroscopy*, ed. J. R. Macdonald, John Wiley& Sons, New York, 1987.

39 A. S. Fouda, H. A. Mostafa, F. El-Taib and G. Y. Elewady, Synergistic influence of iodide ions on the inhibition of corrosion of C-steel in sulphuric acid by some aliphatic amines, *Corros. Sci.*, 2005, **47**, 1988–2004.

40 M. Lebrini, F. Robert, H. Vezin and C. Roos, Electrochemical and quantum chemical studies of some indole derivatives as corrosion inhibitors for C38 steel in molar hydrochloric acid, *Corros. Sci.*, 2010, **52**, 3367–3376.

41 M. A. Migahed, E. G. Zaki and M. M. Shaban, Corrosion control in the tubing steel of oil wells during matrix acidizing operations, *RSC Adv.*, 2016, **6**, 71384–71396.

42 A. S. Fouda, M. A. Ismail, G. Y. EL-ewady and A. S. Abousalem, Evaluation of 4-amidinophenyl-2,2′-bithiophene and its aza-analogue as novel corrosion inhibitors for CS in acidic media: experimental and theoretical study, *J. Mol. Liq.*, 2017, **240**, 372–388.

43 ASTM G3-89, *Standard practice for conventions applicable to electrochemical measurements in corrosion testing*, Annual Book of ASTM Standards, ASTM International, West Conshohocken, 2006.

44 M. Yadav, R. R. Sinha, T. K. Sarkar, I. Bahadur and E. E. Ebenso, Application of new isonicotinamides as a corrosion inhibitor on mild steel in acidic medium: electrochemical, SEM, EDX, AFM and DFT investigations, *J. Mol. Liq.*, 2015, **212**, 686–698.

45 G. Gece and S. Bilgiç, Quantum chemical study of some cyclic nitrogen compounds as corrosion inhibitors of steel in NaCl media, *Corros. Sci.*, 2009, **51**, 1876–1878.

46 A. Mishra, C. Verma, H. Lgaz, V. Srivastava, M. A. Quraishi and E. E. Ebenso, Synthesis, characterization, and corrosion inhibition studies of N-phenyl-benzamides on the acidic corrosion of mild steel: experimental and computational studies, *J. Mol. Liq.*, 2018, **251**, 317–332.

47 M. N. El-Haddad and A. S. Fouda, Corrosion inhibition and adsorption behavior of some azo dye derivatives on carbon steel in acidic medium: synergistic effect of halide ions, *Chem. Eng. Commun.*, 2013, **200**, 1366–1393.

48 M. K. Awad, M. S. Metwally, S. A. Soliman, A. A. El-Zomrawy and M. A. bedair, Experimental and quantum chemical studies of the effect of poly ethylene glycol as corrosion inhibitors of aluminum surface, *J. Ind. Eng. Chem.*, 2014, **20**, 796–808.

49 D. Daoud, T. Douadi, H. Hamani, S. Chafaa and M. Al-Noaimi, Corrosion inhibition of mild steel by two new S-heterocyclic compounds in 1 M HCl: experimental and computational study, *Corros. Sci.*, 2015, **94**, 21–37.

50 P. Kumar, V. Kalia, H. Kumar and H. Dahiya, Corrosion Inhibition for Mild Steel in Acidic Medium by Using Hexadecylamine as Corrosion Inhibitor, *Chem. Sci. Trans.*, 2017, **6**, 497–512.

51 M. N. El-Haddad, A. S. Fouda and H. A. Mostafa, Corrosion inhibition of carbon steel by new thiophene azo dye derivatives in acidic solution, *J. Mater. Eng. Perform.*, 2013, **22**, 2277–2287.

52 A. K. Singh and M. A. Quraishi, The effect of some bis-thiadiazole derivatives on the corrosion of mild steel in hydrochloric acid, *Corros. Sci.*, 2010, **52**, 1373–1385.

53 M. J. Bahrami, S. M. A. Hosseini and P. Pilvar, Experimental and theoretical investigation of organic compounds as inhibitors for mild steel corrosion in sulfuric acid medium, *Corros. Sci.*, 2010, **52**, 2793–2803.

54 E. A. Flores, *et al.*, Sodium phthalamates as corrosion inhibitors for carbon steel in aqueous hydrochloric acid solution, *Corros. Sci.*, 2011, **53**, 3899–3913.

55 A. Zarrouk, B. Hammouti, H. Zarrok, S. S. Al-Deyab and I. Warad, Thermodynamic study of metal corrosion and inhibitor adsorption processes in copper/N-1-naphthylethylenediamine dihydrochloride monomethanolate/nitric acid system: part 2, *Res. Chem. Intermed.*, 2012, **38**, 1655–1668.

56 H. B. Ouici, O. Benali, Y. Harek, L. Larabi, B. Hammouti and A. Guendouzi, Inhibition of mild steel corrosion in 5% HCl solution by 5-(2-hydroxyphenyl)-1,2,4-triazole-3-thione, *Res. Chem. Intermed.*, 2013, **39**, 2777–2793.

57 M. Yadav, U. Sharma and P. Yadav, Corrosion inhibitive properties of some new isatin derivatives on corrosion of N80 steel in 15% HCl, *Int. J. Ind. Chem.*, 2013, **4**, 6.

58 M. A. Quraishi, Thermodynamic and electrochemical investigation of pantoprazole: {(RS)-6-(difluoromethoxy)-2-[(3,4-dimethoxypyridin-2-yl)methylsulfinyl]-1H-benzo[d]-imidazole} as corrosion inhibitor for mild steel in hydrochloric acid solution, *Arabian J. Sci. Eng.*, 2013, **38**, 99–109.

59 O. A. Elgyar, A. M. Ouf, A. El-Hossiany and A. S. Fouda, The Inhibition Action of Viscum Album Extract on the Corrosion of Carbon Steel in Hydrochloric Acid Solution, *Biointerface Res. Appl. Chem.*, 2021, **11**(6), 14344–14358.

60 A. S. Fouda, R. E. Ahmed and A. El-Hossiany, Chemical, Electrochemical and Quantum Chemical Studies for Famotidine Drug as a Safe Corrosion Inhibitor for α-Brass in HCl Solution, *Prot. Met. Phys. Chem. Surf.*, 2021, **57**(2), 398–411.

61 M. Elbelghiti, *et al.*, Experimental, quantum chemical and Monte Carlo simulation studies of 3,5-disubstituted-4-amino-1,2,4-triazoles as corrosion inhibitors on mild steel in acidic medium, *J. Mol. Liq.*, 2016, **218**, 281–293.

62 M. V. D. Linden and J. H. W. DeWit, Corrosion of Al in acidic and neutral solutions, *Electrochim. Acta*, 1993, **38**(14), 1989–1992.

63 N. El Hamdani, R. Fdil, M. Tourabi, C. Jama and F. Bentiss, Alkaloids extract of Retama monosperma (L.) Boiss. seeds

used as novel eco-friendly inhibitor for carbon steel corrosion in 1 M HCl solution: electrochemical and surface studies, *Appl. Surf. Sci.*, 2015, **357**, 1294–1305.

64 G. Sığırcık, D. Yildirim and T. Tüken, Synthesis and inhibitory effect of N,N′-bis(1-phenylethanol) ethylenediamine against steel corrosion in HCl media, *Corros. Sci.*, 2017, **120**, 184–193.

65 E. M. Sherif and S. M. Park, Effects of 1,4-naphthoquinone on aluminum corrosion in 0.50 M sodium chloride solutions, *Electrochim. Acta*, 2006, **51**, 1313–1321.

66 A. S. Fouda, E. Abdel-Latif, H. M. Helal and A. El-Hossiany, Synthesis and Characterization of Some Novel Thiazole Derivatives and Their Applications as Corrosion Inhibitors for Zinc in 1 M Hydrochloric Acid Solution, *Russ. J. Electrochem.*, 2021, **57**(2), 159–171.

67 P. Muthukrishnan, B. Jeyaprabha and P. Prakash, Mild steel corrosion inhibition by aqueous extract of Hyptis Suaveolens leaves, *Int. J. Ind. Chem.*, 2014, **5**, 1–11.

68 A. S. Fouda, M. Abdel Azeem, S. A. Mohamed, A. El-Hossiany and E. El-Desouky, Corrosion Inhibition and Adsorption Behavior of Nerium Oleander Extract on Carbon Steel in Hydrochloric Acid Solution, *Int. J. Electrochem. Sci.*, 2019, **14**, 3932–3948.

69 A. S. Fouda, S. Rashwan, A. El-Hossiany and F. E. El-Morsy, Corrosion inhibition of zinc in hydrochloric acid solution using some organic compounds as eco-friendly inhibitors, *J. Chem., Biol. Phys. Sci.*, 2019, **9**, 001–024.

70 A. S. Fouda, S. A. Abd El-Maksoud, A. El-Hossiany and A. Ibrahim, Effectiveness of Some Organic Compounds as Corrosion Inhibitors for Stainless Steel 201 in 1M HCl: Experimental and Theoretical Studies, *Int. J. Electrochem. Sci.*, 2018, **13**, 9826–9846.

71 Y. Gong, Z. Wang, F. Gao, S. Zhang and H. Li, Synthesis of new benzotriazole derivatives containing carbon chains as the corrosion inhibitors for copper in sodium chloride solution, *Ind. Eng. Chem. Res.*, 2015, **54**, 12242–12253.

72 H. Hamani, T. Douadi, M. Al-Noaimi, S. Issaadi, D. Daoud and S. Chafaa, Electrochemical and quantum chemical studies of some azomethine compounds as corrosion inhibitors for mild steel in 1 M hydrochloric acid, *Corros. Sci.*, 2014, **88**, 234–245.

73 M. Abdallah, Ketamine drug as an inhibitor for the corrosion of 316 stainless steel in 2 M HCl solution, *Int. J. Electrochem. Sci.*, 2019, **14**, 10227–10247.

74 A. Kosari, M. H. Moayed, A. Davoodi, R. Parvizi, M. Momeni, H. Eshghi and H. Moradi, Electrochemical and quantum chemical assessment of two organic compounds from pyridine derivatives as corrosion inhibitors for mild steel in HCl solution under stagnant condition and hydrodynamic flow, *Corros. Sci.*, 2014, **78**, 138–150.

75 A. S. Fouda, S. A. Abd El-Maksoud, A. El-Hossiany and A. Ibrahim, Evolution of the Corrosion-Inhibiting Efficiency of Novel Hydrazine Derivatives against Corrosion of Stainless Steel 201 in Acidic Medium, *Int. J. Electrochem. Sci.*, 2019, **14**, 6045–6064.